UNIVERSITY OF CALIFORNIA
RIVERSIDE

Electrochemical Impedance Spectroscopy Study of Lithium Ion Batteries Combined With Neural Network Modeling and Battery Impedance Analyzing Circuit Design

A Dissertation submitted in partial satisfaction
of the requirements for the degree of

Doctor of Philosophy

in

Materials Science and Engineering

by

Yige Li

December 2019

Dissertation Committee:

Dr. Cengiz S. Ozkan, Co-Chairperson
Dr. Mihrimah Ozkan, Co-Chairperson
Dr. Kambiz Vafai
Dr. Ming Liu

The Dissertation of Yige Li is approved:

_____

_____

_____

Committee Co-Chairperson

_____

Committee Co-Chairperson

University of California, Riverside

Acknowledgments

When I look back my PhD journey, I have so much to thank for. I would like to thank for my principle investigator Dr. Cengiz S. Ozkan and my co-chair Dr. Mihrimah Ozkan for years of instruction and attention. I could not achieve my PhD without you.

I would like to thank for my lab mates Kazi Ahmed, Bo Dong, Zafer Multu, Taner Zerrin, Fabian Villalobos, Daisy Patino, Sandeep Sebastian, Arash Mirjalili, Pedro Pena, Ruoxu Shang, Amirali Akhavi, James Liu, Rachel Ye, Jeffery Bell, Changling Li for invaluable advices, kind hearted lab training and the time we spend together.

I would like to thank for the undergrad team that I worked with for battery management system research: Nickolas Tran, Chris Verdegan, Da Bin Huang, Jake Ongkingco, Darun Seethammagari. I would like to thank for the undergrad team for machine learning project: Xichao Wang, Xia Hua, Jia Xie, Dwaraknath Ravichandran. We couldn't achieve that much without your expertise of computer science engineering. I would like to thank Evan A. Jauregui for explaining chemistry to me. I would like to thank Ran Wang for taking me to NIPS and teach me about neural networks.

Chapter 4 – impedance analyzing circuit is a co-authored work with Jack Gu, Jack Gatfield, Joseph Gozum.from electrical engineering department in University of California, Riverside and professor Roman Chomko in electrical engineering

department as well. The project idea came up by me and was realized by this senior design group. Without them there will not be this prototype. Parts written by them will be marked with their name at the end of each paragraph.

When I look back of this journey, PhD not only prepared me with research skills, but also prepared me with a lot of other skills. Those are independent thinking skills, logic and reasoning, decision making skills, efficient working skills, problem solving skills, learning skills, leadership skills, writing skills, communication skills, effective professional communication skills, emotion control skills, people skills and so on. PhD made me a more rigorous person in thinking. It taught me to make a decision basing on research or data but not intuition.

Last but not the least, I would like to thank for my parents and my brother for your invaluable love and support.

To my parents for all the support.

ABSTRACT OF THE DISSERTATION

Electrochemical Impedance Spectroscopy Study of Lithium Ion Batteries Combined With Neural Network Modeling and Battery Impedance Analyzing Circuit Design

by

Yige Li

Doctor of Philosophy, Graduate Program in Materials Science and Engineering
University of California, Riverside, December 2019
Dr. Cengiz S. Ozkan and Dr. Mihrimah Ozkan, Co-Chairpersons

Lithium ion batteries are widely used in the world. The impedance of lithium ion batteries can potentially give informative insights of battery's life and health if the interpretation of impedance is reliable enough. In this work, the impedance of Panasonic NCA 18650B battery was investigated through electrochemical impedance spectroscopy (EIS) and was modeled using artificial neural network. EIS study shows that under different cycling conditions, such as overcharge and overdischarge, the impedance change of electrolyte, electrode/electrolyte interface of the battery exhibit different behavior. Artificial neural network modeling gives an accurate prediction of battery future impedance for different sections such as equivalent series resistance (ESR), solid electrolyte interface (SEI) and charge transfer resistance, which can be used in battery state of health (SOH) estimation and prediction. Lastly, a design of impedance analysis circuit is given which make it

possible to conduct real time impedance measurement on battery management systems (BMS).

Keywords:

Lithium ion battery, electrochemical impedance spectroscopy, artificial neural network, state of health, battery management systems.

Contents

List of Figures

Chapter 1

Chapter 2

Chapter 3

Chapter 4

List of Tables

Chapter 2

Chapter 3

Appendix

Chapter 1

Introduction and background

1.1 Global environment and market overview

Through the centuries, the world and the society has been going through fast development continuously, driving by everyday industrial revolutions and the advancements of technologies. With the fast advancements and large consumptions, the 21st century leaves human being with big global environmental problems to solve. Such as energy depletion cause by large fossil fuel consumption, global warming caused by excessive carbon dioxide emission and so on.

Energy depletion by definition means that the consumption of energy is faster than the reproduce of energy. Energy can be classified by renewable energy and unrenewable energy. In a certain point, both two types of energy can be faced with depletion.

The energy source of fossil fuels is the one facing depletion, which is one of the biggest problems for human beings in the 21st century. By *BP Statistical Review of World Energy* [1], the year of fossil fuels left is showing in the following chat.

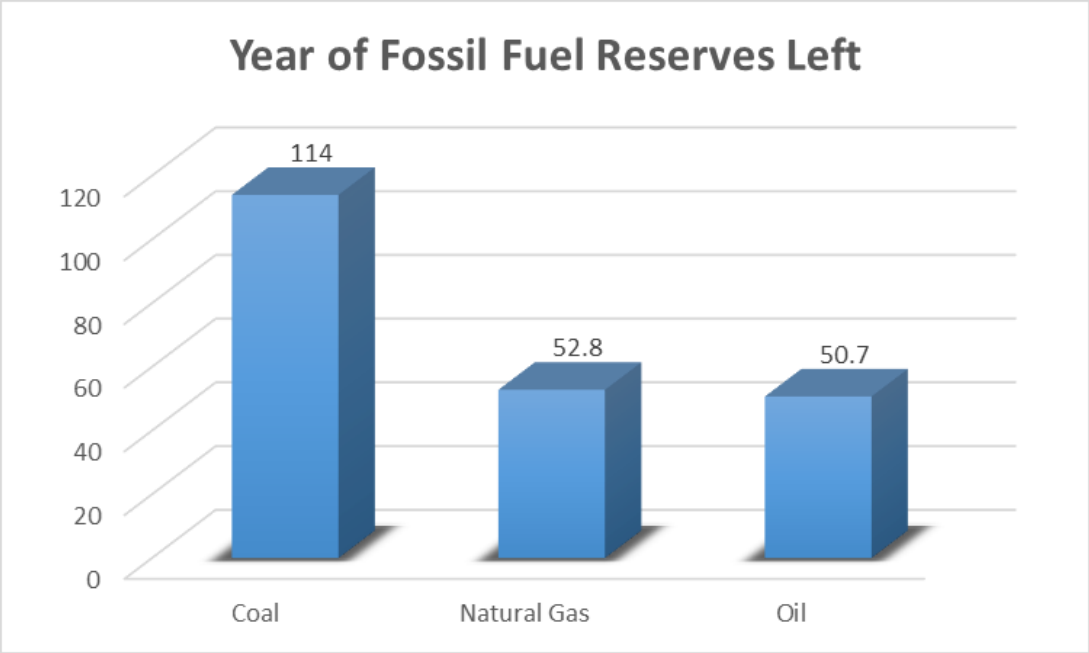

Figure 1. 1 Years of fossil fuel reserves left on earth

Finding energy alternatives for fossil fuel is a necessary and urgent step for human being. Among all solutions, electricity is considered a good alternative renewable energy source. To fully utilize the good of electricity. Improve the performance of energy storage system is a good solution.

Therefore, finding better performance Lithium ion batteries and related studies are being regarded a critical solution for human to face our energy challenges.

1.2 CO_2 emission and global warming

Burning of fossil fuels brings carbon dioxide and other greenhouse gases. Excessive greenhouse gasses in the atmosphere causes global warming and climate change, which have so many effects for the whole natural environments. For example, ice melting worldwide, invasive species dying out, sea level goes up, predictable diseases spreading and animals changing immigration destination and so on [2]. In

California, global warming will bring more droughts and wildfires, native fishes dying out, costal dangers, and spreading diseases [3].

According to *IPCC* [4], the trend of global carbon emission from fossil fuels from 1900 to 2014 is shown in the figure 1.2. As we can see from the figure, carbon emission increases nearly 20 times through 20th century. Therefore, it is a necessary for human to find a solution for excessive carbon emission.

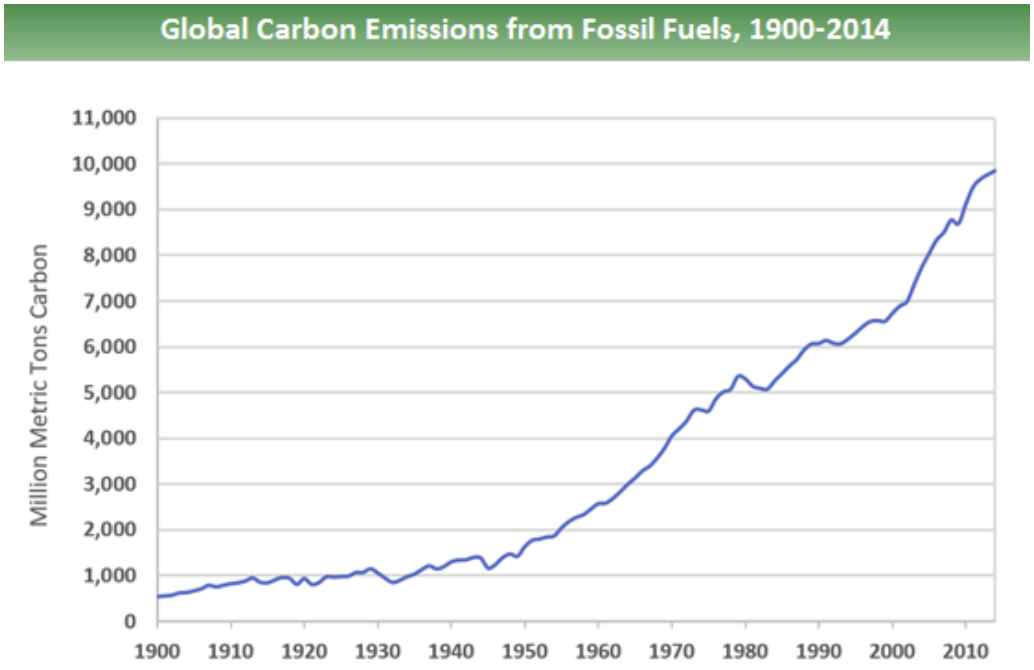

Figure 1. 2 Global carbon emissions from fossil fuels, 1900 - 2014

Low carbon actions are the way of leading us to a solution of the environmental challenges. According to *the union of concerned scientists* [5], there are two ways of solutions people need to follow. One is reducing emissions, and the other one is preparing for impacts. While reduce emissions solves problem existing from beginning which is a more radical way for this problem. Turning renewable energy like solar energy into electricity is considered a cleaner way in the regard of zero

emission. The solution is that rather than burning gasses, coals or other fossil fuels, the production of electricity should be replaced by solar panel, windmills or hydropower. However, to successfully fulfill the process, a reliable energy storage system is very important to perform this mission. Therefore, better performed lithium ion batteries and battery management systems are being considered good solutions to this.

Putting our focus on market level, the growing market of electrical vehicles is being a strong push power for thousands of scientists and engineers to develop a better battery and battery management system. The electric buses sales in China has hugely spiked up from the year of 2014 as shown in the figure 1.3 below, nearly by 100 times [6].

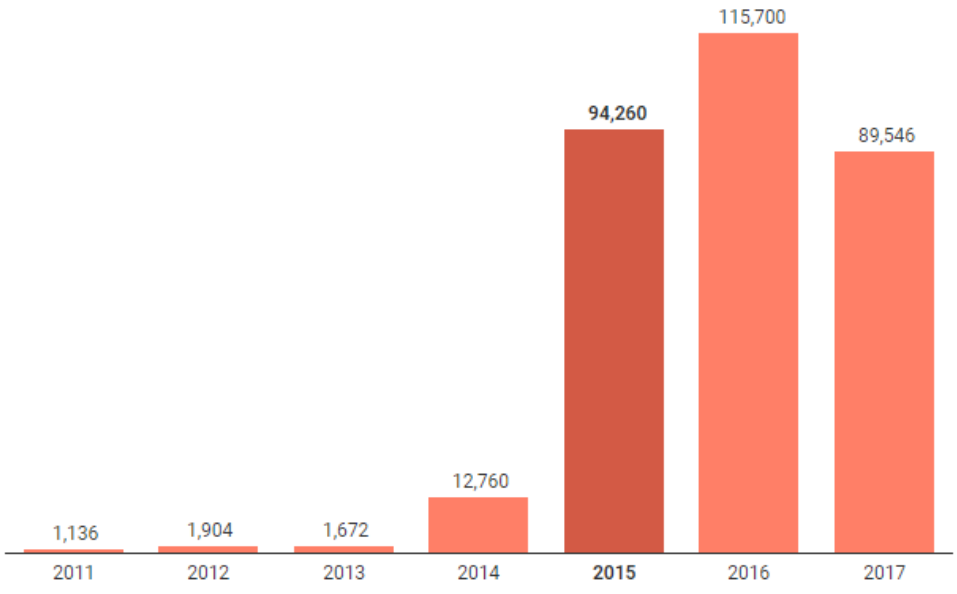

Figure 1. 3 China electric bus sales 2011 - 2017

Moreover, the EV industry worldwide is also growing through the recent years [7]. Therefore, a better performed Battery management system (BMS) is critical to face the challenge of a sustainable energy storage system in EVs.

In summary, considering all of these current situations, the study of lithium ion batteries and lithium ion battery management systems is a necessary route to take to solve these problems.

1.3 Lithium ion battery problems – comprehensive state of health (CSOH) prediction

Lithium-ion battery (LIB) system is one of the most important energy storage systems because of its high energy density and easily convertible chemical energy [8-12]. As impactful developments in LIB capacities and power densities have been made in the recent years, advanced sensing and monitoring technologies are needed in order to predict the battery state of health (SOH) and control the battery operations in advance to avoid any potential safety issues. The internal electrochemical processes of the batteries determine their performances and these electrochemical processes are very difficult to observe since they depend not only on the design and usage of the batteries but also the changes in the ambient environment. Therefore, a comprehensive understanding of the battery characteristics for SOH estimation is crucial in battery management systems (BMS), since this has a big impact on applications such as portable electronics and electric/hybrid vehicles [13,14].

In this regard, researchers have attempted to develop various methods for battery SOH estimation by creating electrochemical models that could enable them to simulate the

behavior of lithium ion batteries. These methods comprise the physical-model approach, which includes the Thevenin model [15], run-time based electrical model [16], and combined electrical model [16,17]. All of these methods provide significant information under nominal conditions and they build a good fundamental understanding of the electrochemical processes. However, unpredictability of the battery internal characteristics due to complex environment conditions makes these models impractical, moreover, most of these models are limited since they treat state of charge (SOC) as the only indicator of SOH by ignoring the effect of degradation inside the cells which could be originating from the interactions between the internal components. SOC is the amount of capacity remaining in a battery compared to its fully charged state. SOH is a notion that serves to compare the performance and health condition of a used battery with a brand new one. However, SOH has not reached a standard definition yet. Researchers and manufacturers use their own definitions for the battery SOH [18 - 22]. Among all of the SOH definitions, there are two kinds that are commonly adopted in the literature. First one is based on the specific capacity values of the batteries. It is defined as $\frac{C_{act}-C_{EOL}}{C_{nom}-C_{EOL}} * 100\%$. C_{act} is the current capacity of a used battery, C_{EOL} is end of life capacity (usually 80% of C_{nom}) of the representative battery, and $C_{nom}$is the capacity of a brand-new battery [18]. A battery may have a large capacity remaining even though its internal resistance is high, which would in turn degrade the performance of the battery. In this case, battery SOH that is based on the capacity will not be accurate. The second group of definition is more comprehensive, which consists of multiple parameters that could reveal a more detailed picture of battery SOH. A. Eddahech *et al.* used a combination of aging

and usage conditions to estimate SOH, where these parameters are used to investigate their related adverse effects on the battery life [19]. Meanwhile, J. Remmlinger *et al.* used the internal resistances as the representative indicators of battery SOH [20]. This second definition of SOH is usually called comprehensive SOH (CSOH). Compared with battery SOH, battery CSOH can give information about battery safety risk, heat generation and other important details [19,20].

Unlike the physical-model approach, another approach focuses on the utilization of the battery data to predict the battery behavior. The so-called data-driven approach includes methods like support vector machine [23], fuzzy logic [24] and neural network [25]. Kalman filtering is also an accepted method which uses the experimental input and output data to find the minimum mean squared error of the true state [26,13]. Data-driven methods are much more flexible than the physical-models since they learn from the history of the system and they are able to predict the future of the system using the historical data. The data-driven methods have been used before, however, the investigation of battery CSOH combined with these methods is relatively rare. Combining the power of data-driven approaches with CSOH analysis could give a much more accurate estimation for the battery behavior. Therefore, using the data-driven methods for battery CSOH estimation is very important. Another benefit of the data-driven methods is their independence from the chemical modeling of the battery, which allows this method to learn the behavior of any type of battery based on the historical data. Gregory L. Plett and his group used Kalman filtering to provide a quantitative estimate of SOH in pack level [27]; Pritpal Singh, et al. developed a fuzzy logic-based

model combined with impedance data to estimate the SOH of the batteries in portable defibrillators, it showed relatively accurate estimation of number of pulses the battery pack could deliver and the remaining cycle life [28]; Githin K. Prasad targeted on two critical indicators, cell resistance and solid phase diffusion time of Li^+, that could determine SOH of the batteries, and then linear least squares algorithms were implemented to produce these parameters for fresh and aged batteries [29].

Among all of the data-driven methods neural network stands out since it can be easily matched with other techniques and it does not need for the detection of model parameters or coefficients since it is performed automatically by training. It is a branch of artificial intelligence that has the capability to deal with a gigantic amount of data. Other significant advantages of neural network include noise tolerance, the ability to deal with incomplete data and non-linear problems. Neural network has also been proven to be a very reliable technique in various practical areas, including medicine, business, renewable energy systems, etc. [30-32]. Using neural network for lithium ion battery applications is particularly advantageous because it is possible to learn battery degradation patterns through impedance behavior from analyzing several batteries and as a result, predictions about future battery behavior can be created.

Electrochemical Impedance Spectroscopy (EIS) is one of the best candidates for CSOH estimation. EIS is an electrochemical characterization technique that can be used for the diagnosis of a wide range of electrochemical systems in order to understand their electrochemical behavior [33,34]. Specifically, EIS can provide detailed information about the interfacial resistances that are experienced within the components of a battery,

namely equivalent series resistance, charge-transfer resistance and solid-electrolyte interphase resistance. The evaluation of the overall impedance, as well as the interfacial resistances of different components in the battery both serve as a guide for any modifications in engineering battery systems to improve their overall electrochemical performance [35]. Besides, EIS is considered to be a technique that can give detailed information of the battery systems without giving any damage to the battery [36]. Another advantage of using impedance as a CSOH indicator is that EIS can be measured in real time within very short time intervals [37,38].

1.4 Basics of Lithium ion Batteries

In this section, the basics and mechanisms of Lithium Ion Battery will be described and demonstrated, which is summarized in the following five sections: definition, configuration, electrochemistry and characterization.

1.4.1 Definition of Lithium Ion Battery

Lithium ion battery is a type of rechargeable battery, also known as secondary battery, in which lithium ions moves between electrode and within electrolyte during charge and discharge process. Lithium ion battery provide outside circuit with electricity during discharge process.

1.4.2 Configuration of Lithium Ion Battery

Within a Lithium Ion Battery cell, anode is usually graphite or prose silicon. Cathode are usually lithium with transition metal oxide. Electrode are usually organic solvent with Lithium ion salt.

During charge process, electrons move from positive electrode to negative electrode

in the outside circuit, and Lithium ions move from cathode to anode within the cell. Process reverses during discharge process. As shown in Fig. 1.4 [39].

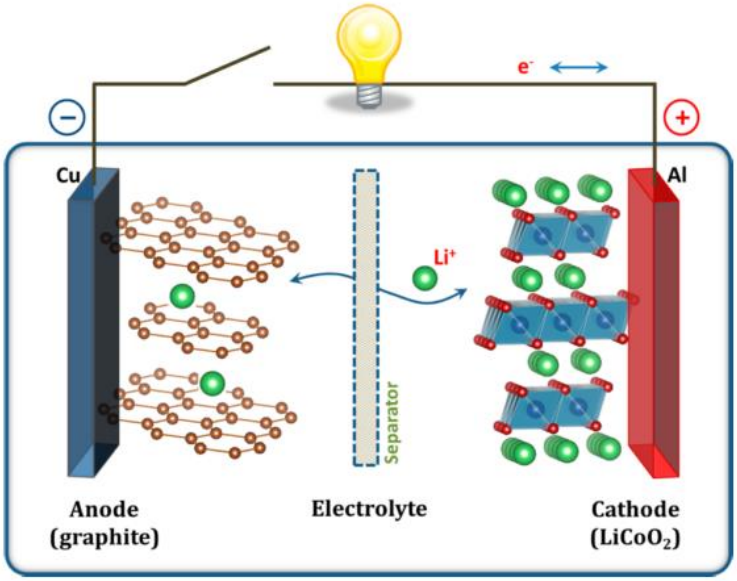

Figure 1. 4 Working Principle of Lithium Ion Battery

Electrochemistry of Lithium Ion Battery

Using LiCoO2 cathode Lithium Ion Battery as an example, chemical reactions of the cell is as following:

Cathode: $CoO_2 + Li^+ + e^- \rightleftharpoons LiCoO_2$

Anode side: $LiC_6 \rightleftharpoons C_6 + Li^+ + e^-$

Overall: $LiC_6 + CoO_2 \rightleftharpoons C_6 + LiCoO_2$

The overall reaction has its limits. Over discharge supersaturates lithium cobalt oxide, leading to the production of lithium oxide, [40] possibly by the following irreversible reaction: $Li^+ + e^- + LiCoO_2 \longrightarrow Li_2O + CoO$

Overcharge up to 5.2 volts leads to the synthesis of cobalt (IV) oxide, as evidenced

by x-ray diffraction [41]: $\mathrm{LiCoO_2} \longrightarrow \mathrm{Li^+} + \mathrm{CoO_2} + \mathrm{e^-}$

1.4.3 Characterizations of Lithium Ion Battery

There are a lot of characterization methods for lithium ion battery, which can be generally classified into two categories: material characterization and device characterization.

For material characterization, SEM (Scanning Electron Microscopy), EDS (Energy Dispersive Spectrum), TEM (Transmission Electron Microscopy), Raman spectroscopy, XRD (X- ray Diffraction) are commonly used methods.

For device characterization, EIS (Electrochemical Impedance Spectroscopy), GITT (Galvanostatic Intermittent Titration Technique), CV (Cyclic Voltammetry) are generally commonly used methods.

1.5 Overview of this work

The topic of this thesis will fall into the area of investigation of Lithium ion batteries. The battery will be talked about most is the commercial NCR 18650 battery.

This work is mainly focusing on testing and characterizations of lithium ion batteries via electrochemical impedance spectroscopy (EIS). As well as battery management systems and machine learning algorithm for battery control.

The problems this work is solving falls on how to improve battery performance through cycling without changing battery chemistries.

In this study we applied a neural network model by using the EIS data, and since the data obtained is plentiful and extensive, this allowed us to make accurate

predictions about the future behavior of the commercial lithium ion batteries. EIS analysis of the lithium ion batteries was performed under several cycling conditions (different SOC, overcharge and overdischarge) to determine CSOH indicators and analyze the impact of different charging profiles on the internal chemical reactions within the cell. Three important CSOH indicators were discussed and the prediction of the future values of these indicators are achieved via a neural network model.

Chapter 2

Electrochemical impedance spectroscopy (EIS) investigations and analyses on lithium ion batteries from different perspectives

2.1 Basics of electrochemical impedance spectroscopy

Mechanisms of electrochemical impedance spectroscopy (EIS) will be mainly introduced in this section for basic understanding and further discussion. Generally speaking, EIS is an impedance measurement technique for electrochemistry systems. During the testing, EIS employ a sinusoidal function of different frequency form mill hertz to kilo hertz in the form of voltage (or current) to the electrochemistry system, and receive the response which is also an sinusoidal wave in the form of current (or voltage). There will be a phase difference between the input signal and the response, which indicate the electrochemistry system is not a pure resistor. And then the impedance of the electrochemistry can be calculated using the equation below:

$$Z(\omega) = \frac{\tilde{V}}{\tilde{I}} = Z_r + jZ_J$$

The impedance contains real part and imaginary part, which is usually be used as X and Y axis in impedance graphs that we most commonly see. As shown in Fig. 2.1.

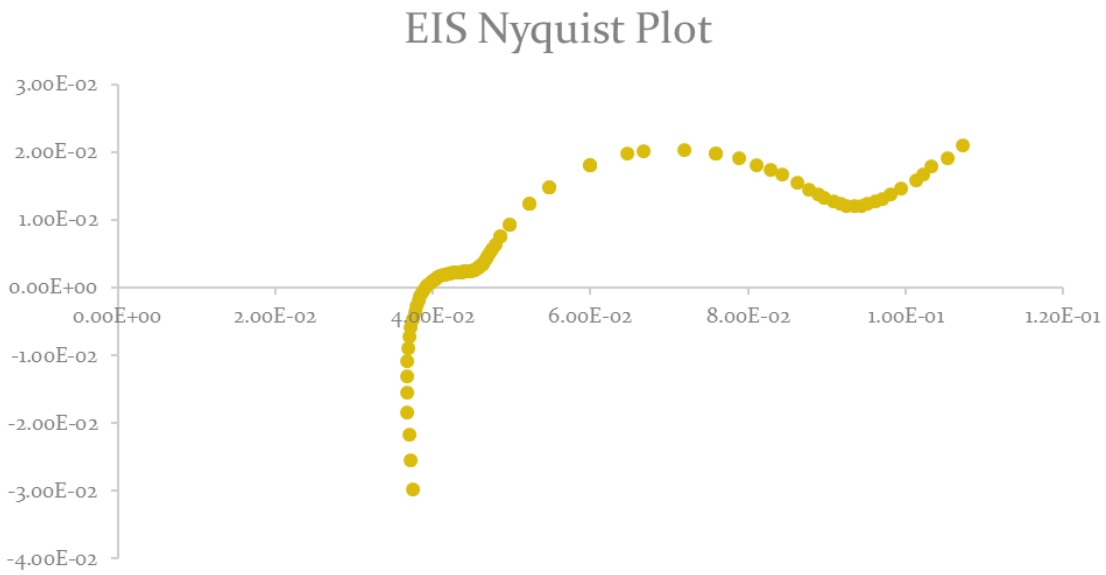

Figure 2. 1 EIS Nyquist Plot

For different electrochemistry systems, the interpretation of semicircles in the impedance diagrams are different, depending on properties of the electrochemistry system.

2.2 Literature research of EIS studies on lithium ion batteries

Electrochemical impedance spectroscopy has been a powerful tool for characterization for different electrochemical systems. In the field of lithium ion battery, EIS is also a powerful tool to investigate the kinetics and aging mechanisms for battery in recent years and the trend is keep going. In 2002, A Hejelm et al [42] give out an EIS analysis of LiMn2O4 cathodes, revealed that the impedance

response is strongly dependent on the current collector used. In 2006, J Jorcin et al [43] gave out CPE (Constant Phase Element) analysis using local EIS, which gives out an fundamental analysis method surface reactivity, surface inhomogeneity, roughness and fractal geometry. In 2008, D Dees et al [44] using EIS to analysis the positive electrode of lithium ion battery, the composition of the electrode is layered nickel oxide ($LiNi_{0.8}Co_{0.15}Al_{0.05}O_2$). The paper also gives out model for the description of oxide – electrolyte interface. In 2011, J Guo et al [45] studied silicon carbon composite anode for lithium ion battery using EIS. This paper gives out an EIS behavior explanation of silicon battery anode in different cycles. In 2013, Z Deng et al [46] analyzed capacity fading of lithium/sulfur battery using EIS. This paper pointed out that charge-transfer resistance is the key factor contribution to the capacity fading of Li/S battery. In 2015, S Erol [47], who is instructed by Dr. Mark Orazem, published thesis paper investigating lithium cobalt oxide/carbon batteries using EIS. This paper gives out a comprehensive analysis of the battery chemistry in different battery condition, such as overcharge, over discharge, different state of charge and temperature.

However, EIS is not a standing alone technique, which means that to conduct a successful EIS analysis, one must be aid with other structural or electrochemical information of the system.

2.3Electrochemistry interpretation

2.3.1 Explanation of the electrochemical analysis through EIS

Electrochemical analysis in this work was based on the basic electrochemical theory explained in this section. Figure 2.2 is a simple scheme of Nyquist plot. It usually consists of all or parts of an inductance tail, one or multiple semi circles, and a diffusion tail that depends on the complexity of the electrochemical systems. Roughly, each part represents a different electrochemistry component that would contribute to the overall impedance of a cell. The details of each electrochemistry component are given in Table 2.1. Such approach has been used to analyze EIS results in various researches on lithium-ion batteries, which was summarized by D. Andre et al [48]. The reason that these parameters can be distinguished into different parts in the Nyquist plot is the significant variation of their time constants [49]. Equivalent series resistance (ESR), charge-transfer resistance (R_{ct}) and solid-electrolyte interphase resistance (R_{sei}) are all important elements that reflect battery health condition under different aging situations. ESR is mainly associated with resistance of the electrolyte and it can reflect the electrolyte consumption, which is related to the degree of irreversible capacity loss of the cell [50,51]. The electrical conductivity of the additives within the electrodes is also contributed to ESR as well [52]. R_{ct} represents the redox reactions happening at the interfaces between the electrolyte and the electrodes during lithiation and delithiation processes [53]. This rate-limiting element is a very sensitive and reliable indicator for surface degradation, especially for ternary cathode materials, including NCA, NMC, LFP, etc. The change of R_{ct} provides significant information about phase transition at the interfaces [54, 55]. R_{sei} is the resistance of the solid-electrolyte interphase (SEI) layer. A stable SEI secures a good capacity of a cell, even though it usually leads to

initial irreversible capacity loss during the wetting and formation cycles [56]. Safety, cycle life and high C-rate performance are directly related to the morphology and quality of the SEI layer, which makes R_{sei} a very significant parameter to be used as an indicator of battery CSOH [57,58]. The exact value of these parameters can be obtained through a fitting procedure introduced in the next section. Since, ESR, R_{ct} and R_{sei} are all important factors that provide useful information on battery health, they are the three indicators we used for CSOH estimation in this work.

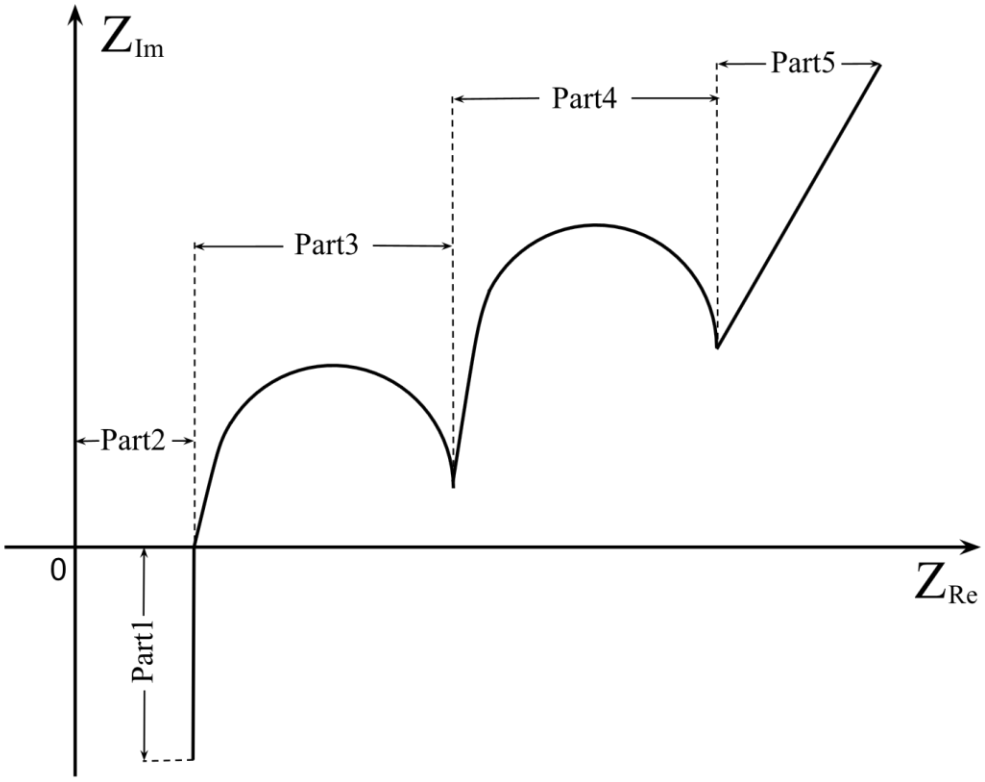

Figure 2. 2 Electrochemistry interpretation of Nyquist plot

Table 2. 1 Electrochemical interpretation of Nyquist plot

Part 1	Inductance	Inductance induced by current collector, wires outside battery
Part 2	Ohmic resistance	Represent as equivalent series resistance
Part 3	SEI resistance and capacitance	Resistance and capacitance of SEI layer
Part 4	Charge transfer resistance and double layer capacitance	Resistance of charge transfer and capacitance of double layer within the cell
Part 5	Diffusion tail	Diffusion process within the cell at low frequencies

2.3.2 Equivalent circuit used for the fitting of EIS data

The fitting of the EIS data was conducted using the embedded software in Bio-Logic BT LAB named ZFit. Fig. 2.3 shows the equivalent circuit (EC) model used to fit the dataset.

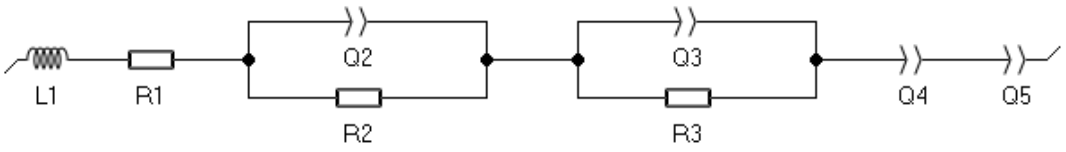

Figure 2. 3 Equivalent circuit (EC) used for Nyquist plot fitting

Based on the basic theory of Nyquist plots [59] and previous works reported by our group [60-62], Equivalent Circuit (EC) shown in Figure 2.3 was selected to fit the

data. This is summarized as follows: Multiple regions related with different components were observed from the Nyquist plots from the EIS measurements of the batteries used in this work. Firstly, at high frequency region, an inductance tail was observed below x axis, thus an inductor was added to the equivalent circuit. Secondly, from all results, two semicircles were observed. In theory, one-time constant result in a perfect semicircle in Nyquist plot [59]. Thus, two time-constant elements were added to the equivalent circuit. Thirdly, the intersect of Nyquist plot with x axis is not zero, which means a resistor has to be connected in series with the whole circuit. Lastly, a tail was observed in the last part of Nyquist plot, which means a capacitor need to be connected with the circuit.

2.4 Study 1 – EIS at different State of Charge of NCR 18650B batteries

2.4.1 NCR 18650B battery and testing conditions

All batteries tested within this paper are 3.7V 3400mAh NCR 18650B lithium-ion batteries from Panasonic company, Japan, as shown in figure 2.4. The chemistry information from the product information sheets is shown in Table 1.

Figure 2. 4 NCR18650 Battery

Table 2. 2 Chemical components of NCR 18650B battery

Component	Material	Formula/CAS*
Positive Electrode	Lithium Cobalt Nickel Aluminum Oxide	$LiCoNiAlO_2$ 193214-24-3
Negative Electrode	Graphite	C 7440-44-0
Electrolyte	Ethylene Carbonate – Solvent	$C_2H_4O_3$ 96-49-1
	Diethyl Carbonate – solvent	$C_5H_{10}O_3$ 105-58-8
	Lithium Hexafluorophosphate – salt	$LiPF_6$ 21324-40-3

*CAS (Chemical Abstract Service)

All batteries were tested by the Bio-Logic Science Instruments Battery Cycler, BCS 815. Cycling data was collected through BT-Lab software that comes with the instrument. The tests were performed under the ambient temperature of the laboratory and the batteries were not kept in any temperature chamber. Thus, temperature fluctuations between day and night are expected.

2.4.2 Testing procedure

Table 3 displays the testing procedure of EIS analysis under different SOCs. Firstly, the capacity check was performed to determine the true capacity of the batteries prior to cycling. This was accomplished with a CC-CV (Constant Current-Constant Voltage) charging and a CC (Constant Current) discharging run for 3 cycles where the average capacity was determined to serve as the real capacity of the battery.

After the capacity check, the batteries were charged with a constant current until they reached a fully charged state at 4.2 V. Afterwards, a constant voltage of 4.2 V was applied to the battery as the reference voltage until the current became equal to or lower than 50 mA. After this point, the batteries were discharged at 320 mA for 1 hour and then they were set to rest for 1 hour. It was during this resting period that the open circuit voltage was recorded, and then EIS measurements were conducted. Lastly, the batteries were discharged at 320 mA for 1 hour again. This entire process was repeated 9 more times till the battery is fully discharged. For the EIS measurements, a voltage with an amplitude of 5 mV was applied between a frequency range of 10 mHz - 10 kHz.

Table 2. 3 Experimental setting testing profile

Capacity check (loop for 3 cycles in total)	Charge: CC-CV	Current = 1150 mA, Voltage = 4.2 V, End Current = 50 mA
	Discharge: CC	Current = 460 mA, End Voltage = 3.0 V
Testing	Discharge: CC	Discharge 320mA for 1 hour and EIS (Run for 10 loops)
	Charge: CC	Charge 320mA for 1 hour and EIS (Run for 10 loops)

2.4.3 Nyquist plots and discussions

Figure 2.5 displays the Nyquist plots for discharge and charge at SOCs of 10%, 60% and 100%. For both discharge and charge processes, it can be seen that at both 10%

and 100% SOC, plots display two semi-circles, while at 60% SOC, there is only one semi-circle. Number of the semicircles along with various parameters were obtained from the Nyquist plots at different states of discharge and charge and they are listed in Table 4. It was seen from the Nyquist plots that for the discharging process, two semicircles formed up at 100% SOC. However, from 90% SOC to 30% SOC, only one semi-circle was observed and at 20% SOC the two semicircles appeared again and continued showing up until the battery was fully discharged at 0% SOC. The charging process has a similar trend. Two semicircles were observed from 0% SOC to 20% SOC. At 30% SOC, the semicircle merging phenomenon was observed, and a single semicircle was seen from 40% SOC to 80% SOC. At 90%, the semicircle merging phenomenon was presented again and lastly 2 semicircles were observed when the battery was fully charged at 100% SOC. A similar phenomenon was also observed in other studies on the same type of battery [48]. This phenomenon could be explained by the increase in charge-transfer resistance near terminal SOCs. The semicircles showing up at terminal SOCs represent the charge-transfer resistance, while the semi-circles showing up during the whole SOC sweep is SEI resistance. When the battery is near fully charged or discharged states, compared with more neutral SOC cases, the lithium ions experience a greater “resistance” to migrate into electrode when applied voltage since there is already a high lithium ion concentration presence at the electrode near terminal SOCs.

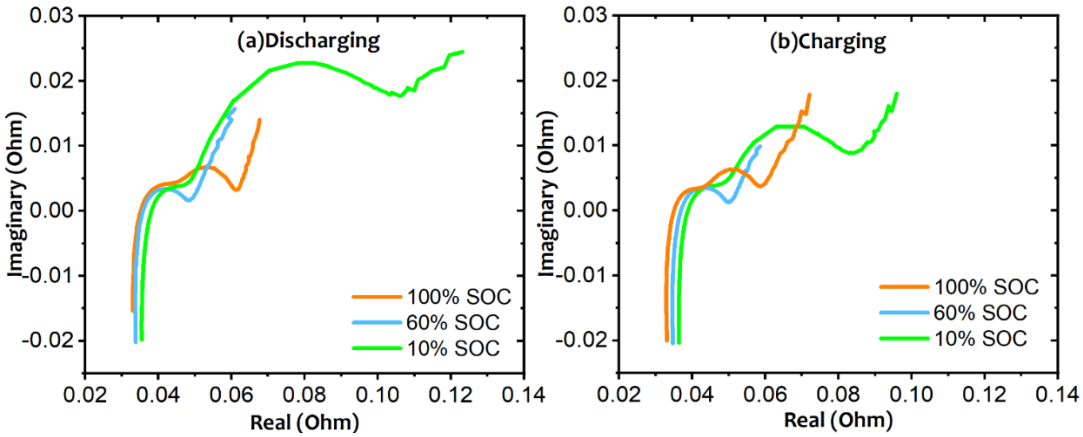

Figure 2. 5 Nyquist plot for (a) discharging and (b) charging process at 10%, 60% and 100% SOC respectively. (a) and (b) are with same scale.

Table 2. 4 Values of SOC (state of charge), and its corresponding OCV (open circuit voltage), battery charge and number of observable semicircles on Nyquist plot for discharging and charging processes

	Discharging (c-rate: C/10)										
SOC (state of charge/%)	100	90	80	70	60	50	40	30	20	10	0
OCV (open circuit voltage/V)	4.06	3.95	3.87	3.77	3.66	3.60	3.54	3.44	3.33	3.05	2.99
Battery charge (mA*h)	3200	2880	2560	2240	1920	1600	1280	960	640	320	0
# of semi-circles on Nyquist plot*	2	1	1	1	1	1	1	1	2	2	2

	Charging (c-rate: C/10)										
SOC (state of charge/%)	0	10	20	30	40	50	60	70	80	90	100
OCV (open circuit voltage/V)	3.38	3.51	3.58	3.63	3.71	3.82	3.90	4.00	4.11	4.25	4.27
Battery charge (mA*h)	0	320	640	960	1280	1600	1920	2240	2560	2880	3200
# of semi-circles on Nyquist plot*	2	2	2	merge	1	1	1	1	1	merge	2

* number of semi-circles on Nyquist plot here means semi-circle observable by human eyes on Nyquist plot of each SOC.

2.4.4 Fitting results and discussions

After data fitting, the values of ESR, R_{sei} and R_{ct} were determined as shown in Figure 2.6 ESR is the resistor component shown as R1 in the EC model. Similarly,

R_{sei} is the resistor component shown as R2 and R_{ct} is the resistor component shown as R3 in the EC model. R_{sei} is more stable through different SOCs, while R_{ct} values have a "dent" behavior within the whole SOC sweep. During discharge, the charge-transfer resistance does not change much until 40 % SOC, then it gradually increases after the battery is drained to a SOC of 30%. The reason of the increase in charge-transfer resistance near the terminal voltage was explained in the previous section (3.1.2). This behavior is observed solely for discharging and is absent during charging, because the terminal voltage for discharging is smaller compared to the terminal voltage for charging, resulting in a larger charge-transfer resistance near 0% SOC during the discharge process compared to the charge process. ESR is stable during both discharge and recharge, as its value remains almost constant at different SOCs. This means that the resistance of the electrolyte does not significantly change within one cycle, indicating the absence of any electrolyte consumption within that cycle. R_{sei} first decreases when the battery starts discharging and it reaches a minimum when the SOC is ~80%, then it keeps increasing until the battery is fully discharged. During charging, a similar trend is observed. R_{sei} decreases to its minimum when the SOC is ~40%, then it keeps increasing until the battery is fully charged. This behavior could be explained as follows. During discharge, the SEI layer first decomposes on anode, and then it forms on the cathode. During charge, the SEI layer first decomposes on the cathode and then it forms on the anode [56]. The result that R_{sei} reaches its minimum at 80% SOC during discharge, while it reaches its minimum at 40% SOC during recharge indicates that the formation of SEI is slower than the decomposition of SEI. Based

on the tests under different SOCs, we can reach to the conclusion that EIS behavior is most distinct under fully charged and fully discharged states. Therefore, the EIS measurement is performed at fully charged states for the following experiments.

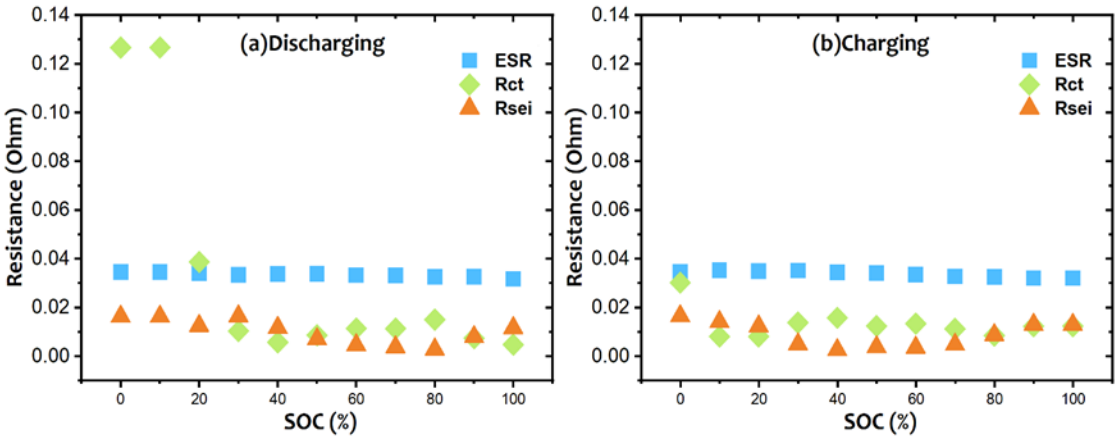

Figure 2. 6 Equivalent circuit fitted results of (a) discharging and (b) charging testing results. (ESR – equivelant series resistance, Rsei – solid electrolyte interface resistance and Rct – charge transfer resistance)

2.5 Study 2 – EIS analysis under overcharge and overdischarge of NCR 18650B batteries

2.5.1 Testing procedure

Same battery as in study 1 was used in this study for testing.

Since the variation of impedance for commercial lithium ion battery is not very significant during standard cycling, overcharge and over discharge tests were designed to find out the CSOH indicators through impedance analysis. The testing procedure can be found in Table 5. Four groups of measurements were performed, where all four groups underwent 3 cycles of slow rate cycling (680mA) and 6 cycles of fast rate cycling (6800mA), followed by repeating the test from the beginning for 6-

10 times. EIS measurements were recorded at fully charged states of every cycle. The fully charged terminal voltages were raised from 4.2V to 4.3V for overcharge testing and fully discharged terminal voltages were lowered from 2.5V to 2.3V for overdischarge testing. For the EIS measurements, a voltage with an amplitude of 10 mV was applied between a frequency range of 10 mHz - 10 kHz.

Table 2. 5 Cycling Profile for Four Groups of Studies

	Normal charge normal discharge	**Normal charge Overdischarge**	**Overcharge Normal discharge**	**Overcharge Overdischarge**
Step 1 slow cycling for 3 cycles	CC charge to 4.2V 680mA EIS CC discharge to 2.5V 680mA	CC charge to 4.2V 680mA EIS CC discharge to 2.3V 680mA	CC charge to 4.3V 680mA EIS CC discharge to 2.5V 680mA	CC charge to 4.3V 680mA EIS CC discharge to 2.3V 680mA
Step 2 fast cycling for 6 cycles	CC charge to 4.2V 6800mA CC discharge to 2.5V 6800mA	CC charge to 4.2V 6800mA CC discharge to 2.3V 6800mA	CC charge to 4.3V 6800mA CC discharge to 2.5V 6800mA	CC charge to 4.3V 6800mA CC discharge to 2.3V 6800mA
Loop	Loop to step 1 and repeat tests			

2.5.2 Nyquist plots

Figure 2.7 shows the Nyquist plots for four different groups of tests. At the first glance, it can be seen that the overall impedance values tend to increase gradually with the cycle number. As the cycle number increases, Nyquist plots are shifting right much faster in Figure 2.7(b) compared to those in Figure 2.7(a). The shifting phenomenon is even greater in Figures 2.7(c) and (d) compared to the shifts in Figures 2.7(a) and (b). This is due to the increase of ESR since the right shift of the Nyquist plots originates from the increase of the real part of the impedance. The reason of this increase will be explained in the next section after data fitting. Comparing Figures 2.7(a),(b) with Figures 2.7(c),(d), it can also be seen that the second semi-circles are larger in Figures 2.7(c) and 5(d), which is partially due to the fact that EIS measurement voltage for Figures 2.7(c),(d) is 4.3V, whereas it is 4.2V for Figures 2.7(a),(b). Besides, for the groups in Figures 2.7(a) and (b), we observe a larger impedance in the 0^{th} cycle compared to the 18^{th} cycle. This is commonly seen in lithium ion battery systems and it is caused by various reasons such as oxygen vacancy formation and activation in the electrochemistry system during the first cycle [63].

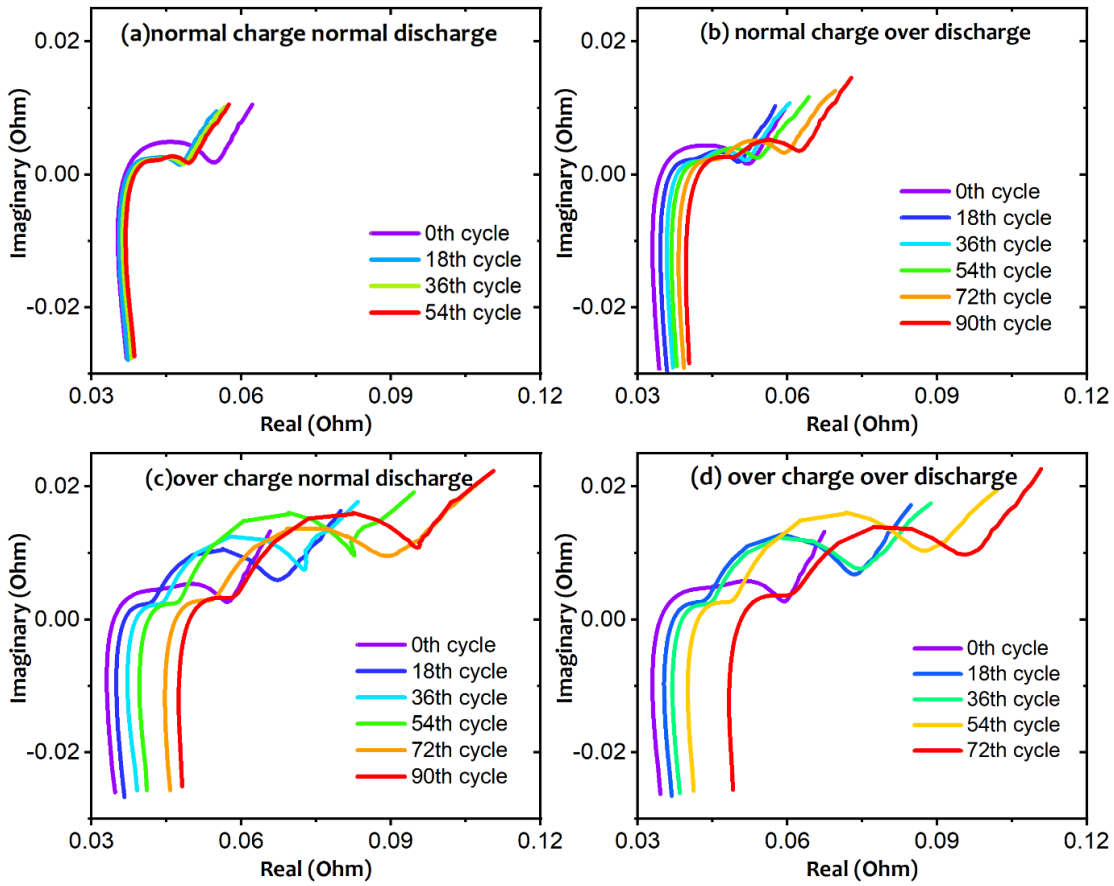

Figure 2. 7 Nyquist plot of electrochemical impedance spectroscopy measurement at fully charged state of four group of tests (a) normal charge normal discharge (b) normal charge overdischarge (c) overcharge normal discharge (d) overcharge overdischarge, respectively. Four plots are using same scale.

2.5.3 Fitting results

Figure 2.8 shows the fitted results for the four different groups of tests. From Figure 2.8, it can be seen that different battery cycling profiles will lead ESR, R_{ct} and R_{sei} change differently through cycling. ESR remains stable for normal charge/normal recharge group as seen in Figure 2.8(a), but it slowly increases for normal charge/overdischarge group as seen in Figure 2.8(b). However, the increase of ESR throughout cycling is much more rapid for overcharge/normal discharge group (Figure 2.8c) and overcharge/overdischarge group (Figure 2.8d). This indicates that

the negative effect of overcharging process on the electrolyte resistance is more pronounced than that of overdischarging. This may be due to the cobalt dissolution from the cathode into the electrolyte with higher cut-off voltages, which has been reported in studies with similar cobalt oxide-based cathodes [50,51]. R_{sei} is stable in Figures 2.8(a) and (b). For Figures 2.8(c) and (d), R_{sei} does not change much at the beginning but it increases after ~50 cycles. This could mean that SEI layer is stable for the groups in Figures 2.8(a) and 2.8(b) and it starts to grow thicker after several cycles for the groups in Figures 2.8(c) and 2.8(d). R_{ct} increases very slowly for the groups in Figures 2.8(a) and 2.8(b) and it increases much faster for the groups in Figures 2.8(c) and 2.8(d) as the cycle number increases. In general, the increase of R_{ct} during cycling is due to the degradation of the holding structures (frame) of both the cathode and the anode resulting from the changes in the microstructure of electrode materials caused by the intercalation/deintercalation of lithium ions. This effect is very common since more reaction sites will be passivated with the increase of cycle number and the continuous formation of SEI layers due to side reactions will also decrease the redox reaction rate.

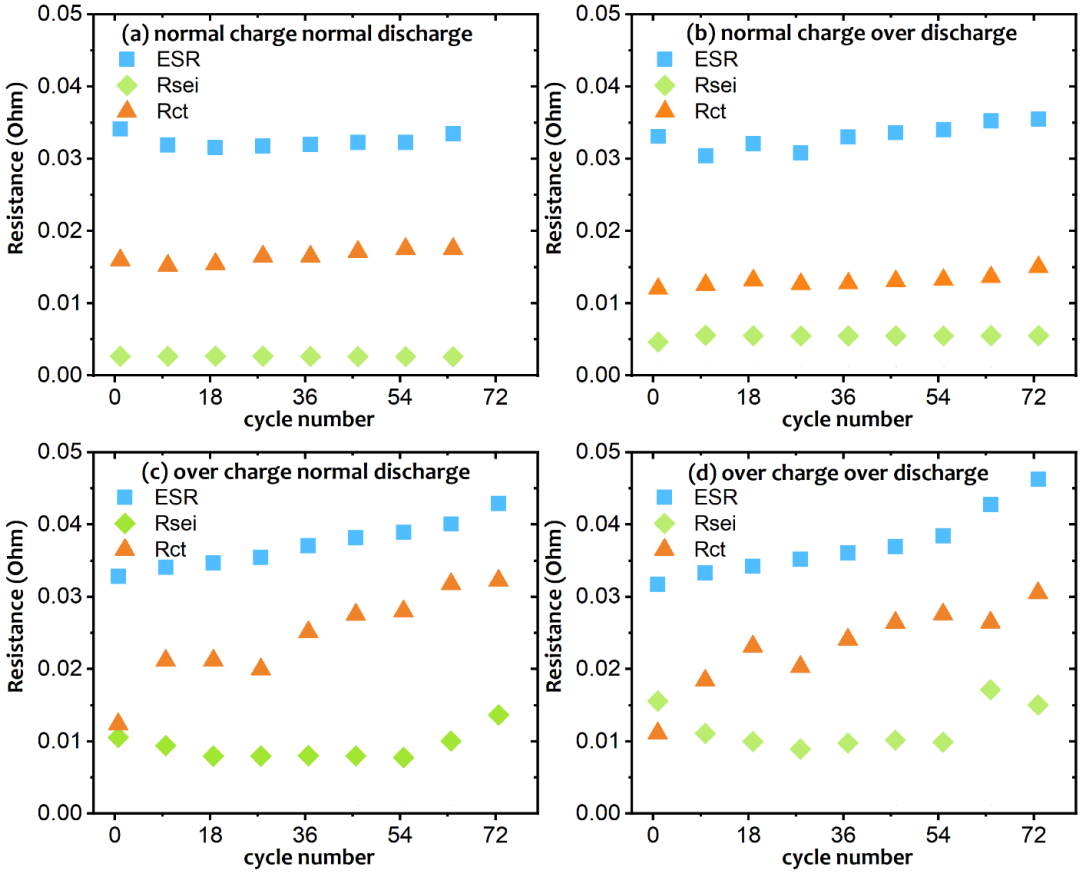

Figure 2. 8 Equivalent circuit fitted results of Nyquist plots of four group of tests (a) normal charge normal discharge (b) normal charge overdischarge (c) overcharge normal discharge (d) overcharge overdischarge, respectively. (ESR – equivelant series resistance, Rsei – solid electrolyte interface resistance and Rct – charge transfer resistance)

2.6 Study 3 – EIS under Different cycling profiles of NCR 18650B batteries

Herein, we investigated the performance of Panasonic NCR18650B battery in regular cycling, fast charging, rest in charge state and shelf life testing using an optimized equivalent circuit model in EIS fitting. NCR 18650B battery, already commercially used in TESLA EV and many other portable electronics, still lack of global understanding of aging in real time. We employ electrochemical impedance

spectroscopy (EIS) as a primary technique. With the choosing of highly accurate equivalent circuit in fitting, and better key factor and indicator in aging, we are allowed to observe the electrochemical phenomena within the cell dynamically and much more in detail.

Testing of EIS of Panasonic NCR18650 Battery in different cycling conditions/profiles: regular cycling, fast charging, rest in charge state, rest at nominal voltage.

Find a suitable and accurate equivalent circuit to fit EIS data (Nyquist plot) and get the evolution of resistance and capacitance in different parts of battery.

Find out the dominance changing factor(s) in different battery cycling process and make comment on how battery cycling methods influence the performances of battery.

2.6.1 Testing procedure

Same battery as in study 1 was used in this study for testing.

Four groups of tests were run, and it is shown as below:

C/10 cycling: C/10 charge and discharge;

C/5.84: C/5.84 for charge; C/10 for discharge;

Rest in high voltage: Rest for two hours between C/10 cycling for charge and discharge;

Shelf life (Store battery): Rest at nominal voltage.

2.6.2 Fitted Results

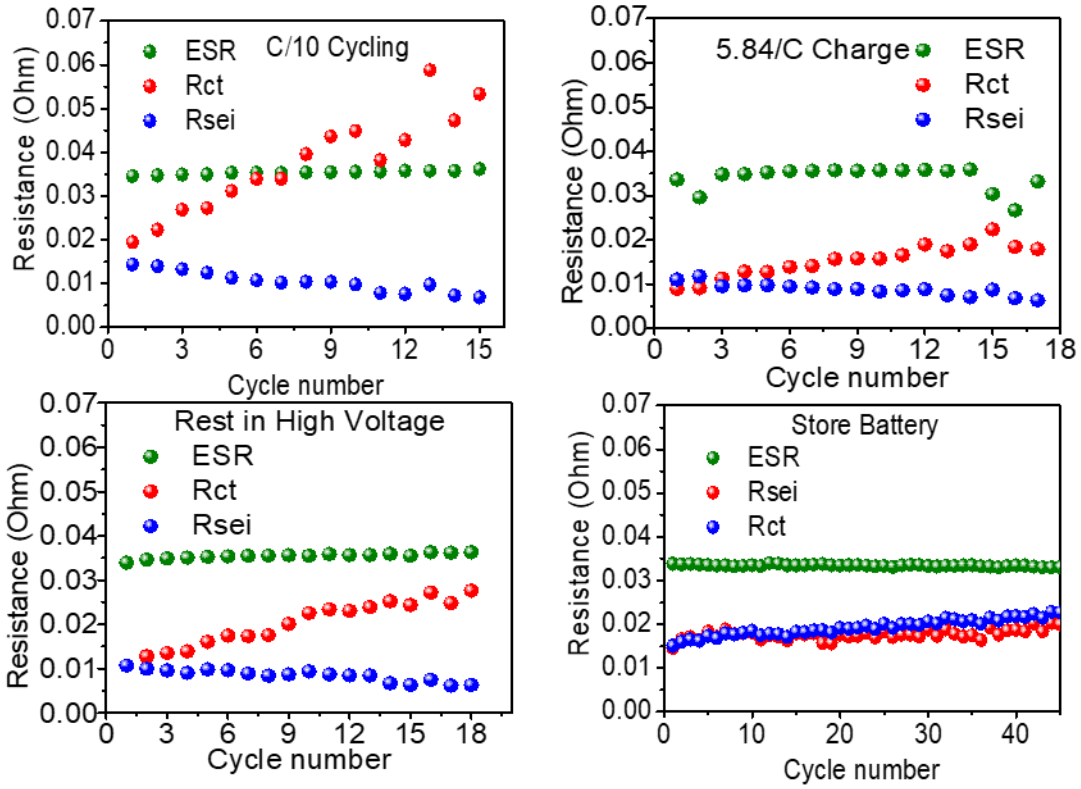

Figure 2. 9 EIS Fitted Results for C/10 cycling, 5.84/C charge, rest in high voltage, and store battery

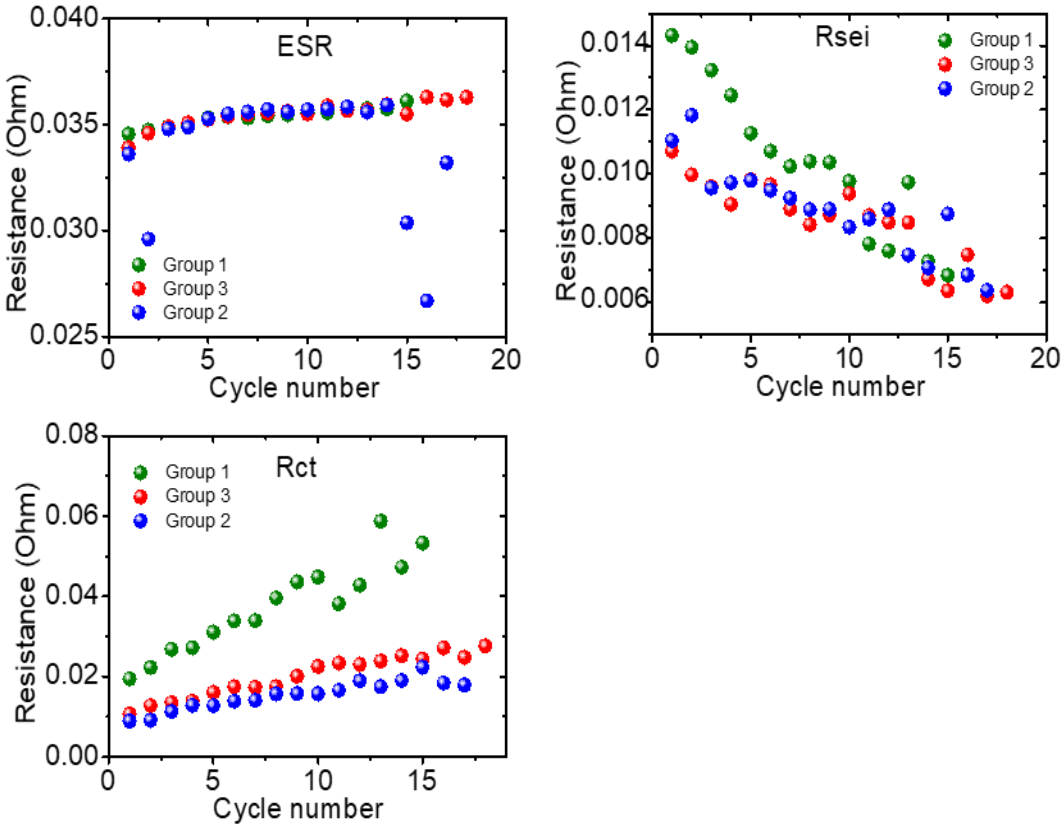

Figure 2. 10 EIS Fitted Results for ESR, Rsei and Rct

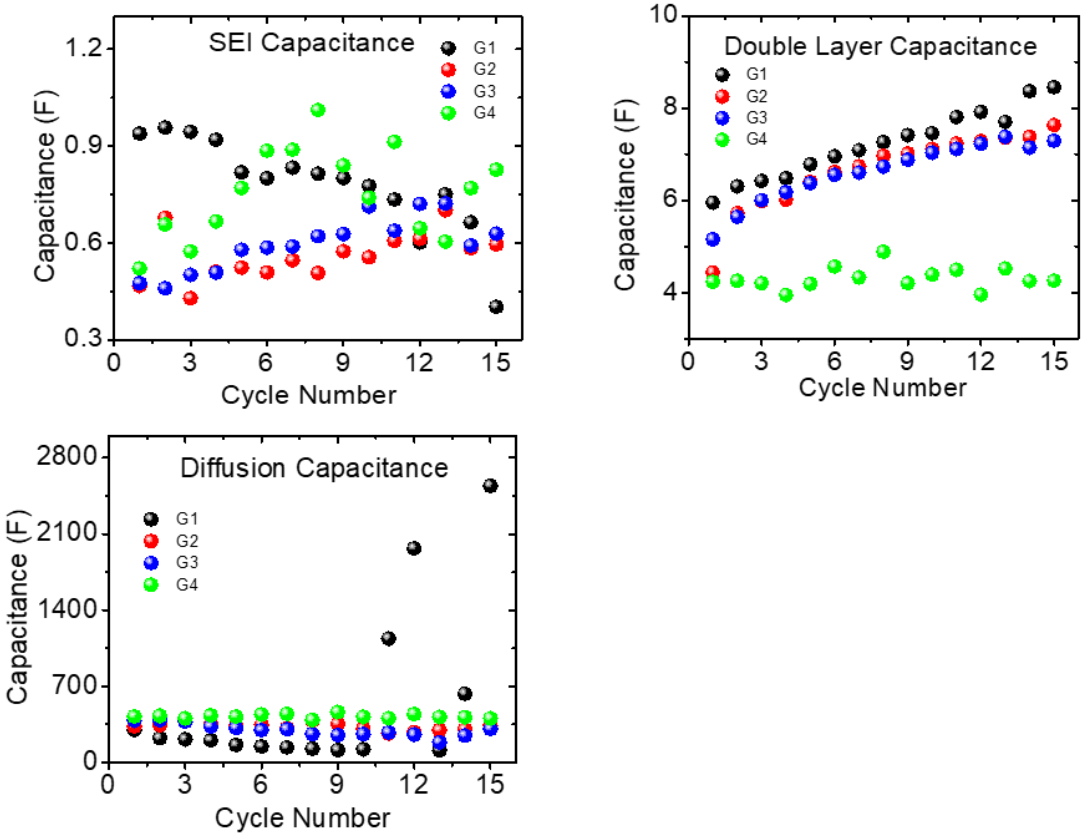

Figure 2. 11 EIS Fitted Results for SEI capacitance, double layer capacitance and diffusion capacitance

2.7 Study 4 – Silicon anode aging with different conditioning study using EIS

2.7.1 Introduction of silicon anode lithium ion battery

Among the substitution of graphite for anode materials, Silicon has been regarded as a promising material which has a high theoretical specific capacity. Many works have done with Silicon anode LIB through the years [64]. However, the mechanism of the formation of SEI layer in Silicon anode is still unclear in the field of research.

Usually, during the first few cycles of charging and discharging of LIBs, SEI layer forms on the anode of battery. The formation of a stable SEI layer during the first few cycles of a lithium-ion cell is critical to the cell's lifetime, performance, and safety. A stable SEI isolates the electrode surface from the electrolyte, which would otherwise undergo irreversible and parasitic side-reactions under the existing difference in potential between the two phases. The investigation of SEI formation in variety of battery systems has attracted a lot of interest. M. B. Pinson et al came up with a theoretical model to describe the formation process of SEI [65]. However, more experimental data is still needed to further explain and describe the process and to validate existing theories. Recently, EIS has become a popular technique to investigate battery systems [66-68], which has the ability to scope different chemistry parts within battery. Different frequency region represents different chemistry inside of battery. Herein, we employ EIS as a primary technique to i6nvestigate the formation of this interphase on lithium-ion anode in half-cell configuration. EIS allows us to observe the impedance and associated time constant of the SEI layer in-situ in isolation from other electrochemical phenomena within the cell.

2.7.2 Experimental

For the purpose of this investigation, we used half-cells assembled in coin cell form. Silicon was chosen as working electrode and Li metal chips were used as the counter electrode. 1M solution of lithium hexafluorophosphate (LiPF6) in 1:1 volume ratio of FEC:PC solvent was used as electrolyte.

Testing was employed by Bio-logic BCS (Battery Cycling System) - 810. We divide

the tests into two groups. Group 1 and group 2. Both groups are in constant current profile. Group 1 cycles at a rate of C/50 meanwhile group 2 cycles at a rate of C/100. After 3 cycles of slow charging/discharging to ensure the formation of a stable SEI layer, cycling currents are switched to faster charging/discharging at a rate of C/10. EIS data was collected every five hours during the initial slow cycling stage and was later collected at the beginning of every subsequent normal cycle.

To analyze the experimental EIS data, we used equivalent circuit shown in figure 2.12 as model to fit the data. The circuit consists of resistors and constant phase elements (CPEs). The latter represent spatially non-uniform capacitances and have an associated ideality factor. We export experimental data into an excel file which has the model built in and fitted the data by hand.

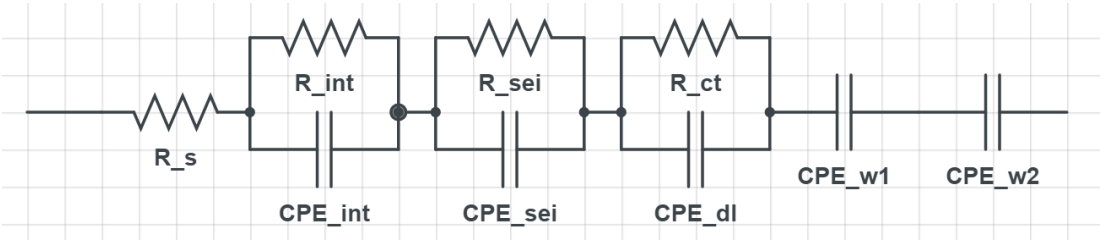

Figure 2. 12 Equivalent circuit used for silicon anode lithium ion battery modeling

Here in the equivalent circuit, RS represents electrolyte resistance, RINT represents internal electronic resistance of conductive network within electrode material, CPEINT represents associated capacitance arising from finite conductivity of electrode material. RSEI represents the resistance of SEI layer. CPESEI represents the capacitance of SEI layer. RCT determines the reaction rate for the lithiation/delithiation processes. CPEDL represents the capacitance of the double layer formed at the electrode-electrolyte interface. CPEW2 represents the

capacitance associated with concentration gradient built up during diffusion of lithium ions in the electrolyte near the electrode surface. CPEW1 represents the capacitance associated with diffusion within the solid electrode matrix.

2.7.3 Results

EIS plots

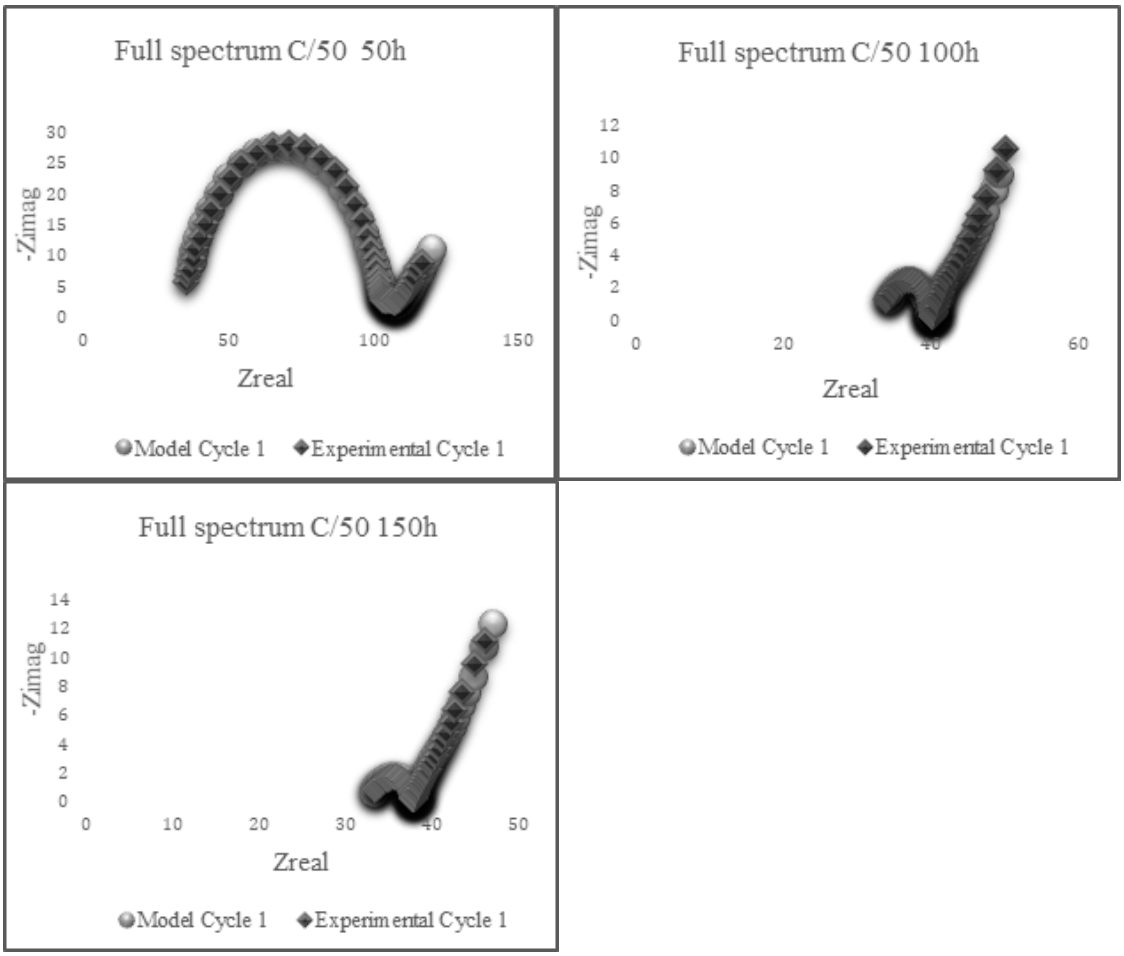

Figure 2. 13 EIS plot of group 1 in 50h, 110h and 150h

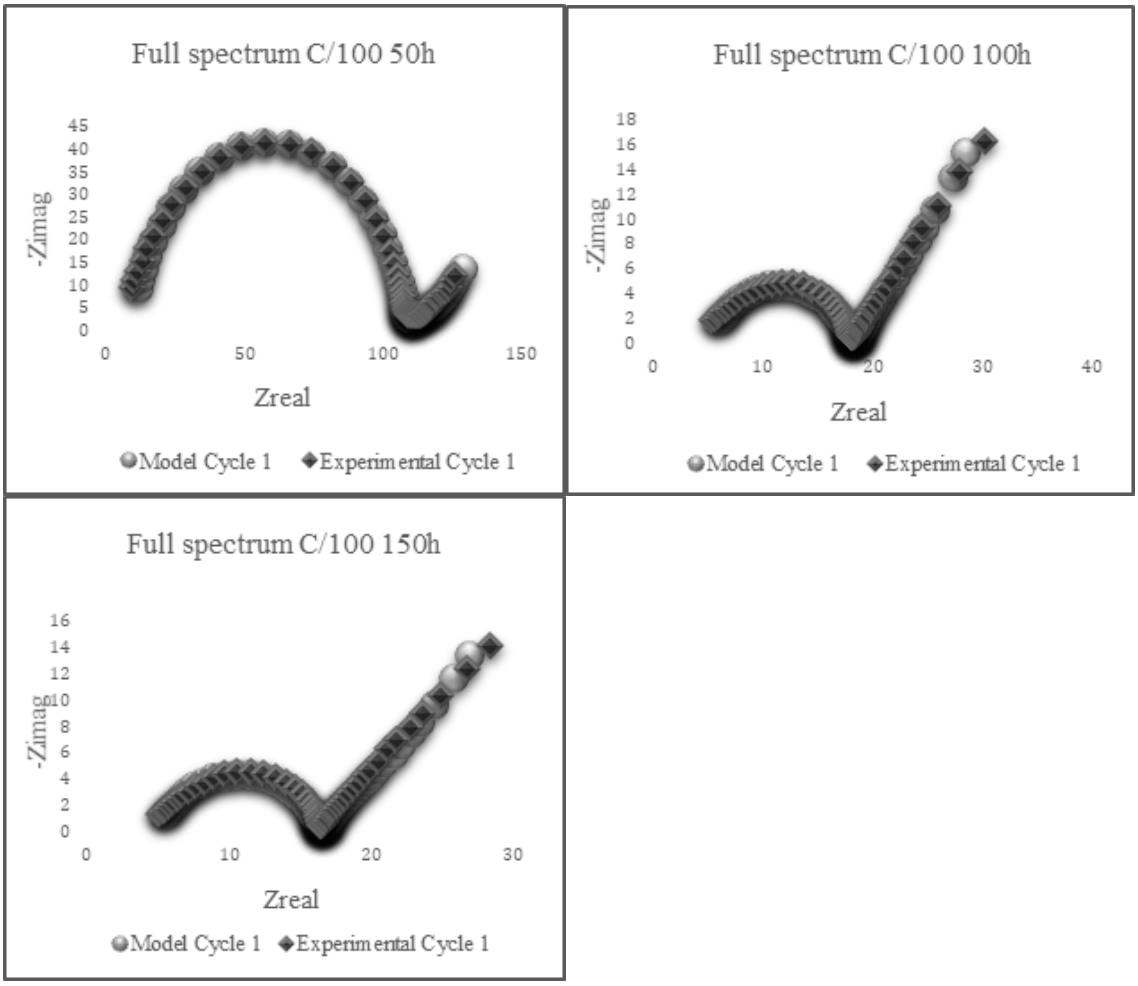

Figure 2. 14 EIS plot of group 2 in 50h, 100h and 150h

Resistance data draw from fitting

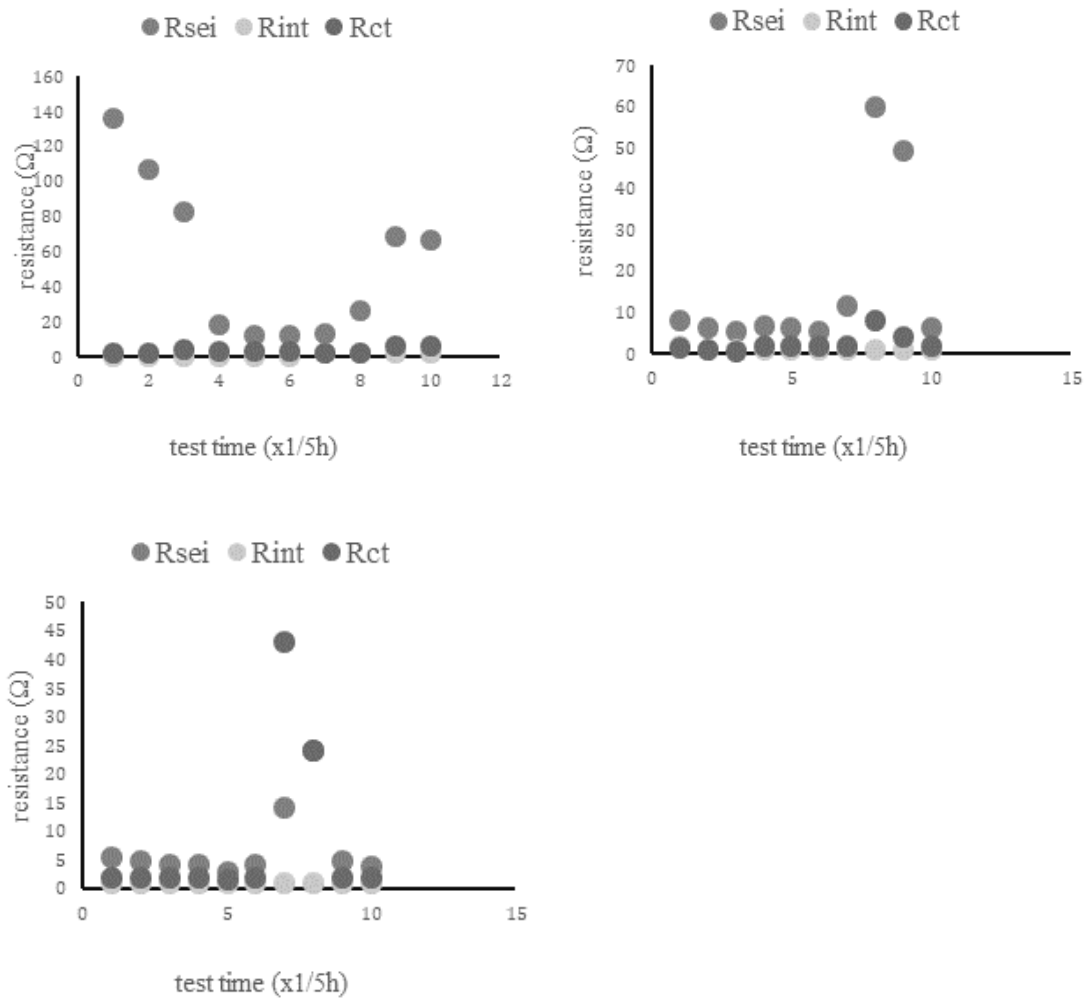

Figure 2. 15 Resistance (Rsei, Rint and Rct) through the time of group 1

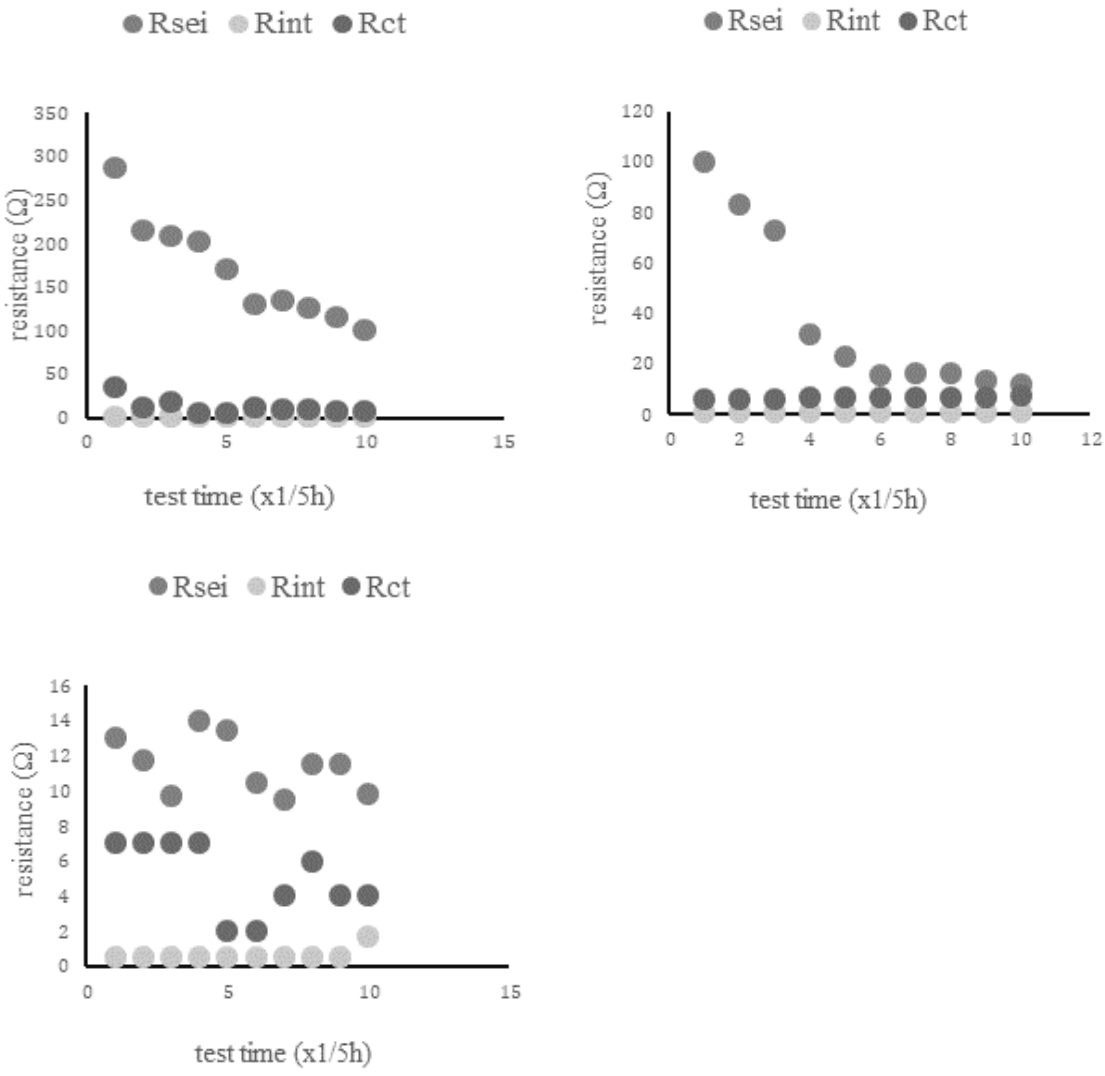

Figure 2. 16 Resistance (Rsei, Rint and Rct) through the time of group 2

2.7.4 Discussions and Conclusions

EIS data has been collected with C/50 and C/100 profile in the initial cycles of Si anode battery. A suitable and practical equivalent circuit has been proposed to fit the impedance data.

Results shows that in a lower C rate, the SEI layer forms slower. During the slow

cycling of battery, the resistance of SEI also varies with the charge and discharge. Based on that, we can control the speed of SEI formation by employ a lower C rate. Besides, the resistance of SEI is much larger than the resistance of contact part and internal resistance. Further trends show that group 2 have better results. Based on that we can compare Si anode Li-ion battery with other Li-ion batteries. However, results is done by hand fitting, the precision is still need to be improved. Besides, more normal cycles will be fitted in the future to see which slow charging/discharging profile is more suitable to form a stable SEI layer.

In a long run, considering the safety of battery, reduce impedance is the direction of effort. The small the impedance, the better the data. In that aspect, group 2 is more promising to make a battery.

Chapter 3

Battery state of health prediction using neural network model

3.1 Introduction of neural network

3.1.1 Neural network modeling and the algorithm

Neural networks (NN), or artificial neural networks (ANN), are series of algorithms or models which imitate the computational process that occurs within the human brain to process the data obtained from computer. Neural networks are the attempts of humans to recreate natural neural networks found in living organisms. They work by taking in large amounts of raw data and then recognizing the patterns that lie within the data, clustering data with similarities together. To do this, the user defines sets of known inputs and outputs, typically in the form of arrays of numbers. It searches for patterns between the inputs and outputs, and uses the information acquired to make predictions on future outputs. The larger the data set available to train the neural network, the more accurate the predictions become. ANN have become the center of deep learning and today they are being used for tasks such as

classifying images, speech recognition, objection detections, etc. [69]. The reason that we used neural network as the method for battery SOH prediction is because it yields out the highest accuracy compared with different adaptive methods for SOH estimation, such as Kalman filter and fuzzy logic. [13]. ANN used in this paper is a supervised learning process. Fig. 3.1 demonstrates how this training process works. A weight function is assigned between inputs and output. Usually, outputs are a weight sum of inputs. Output is compared with the ground data and an offset is obtained. Weights are updated every time using the offset and the back-propagation method. Weights will be updated during the training loop until the error/offset is small enough.

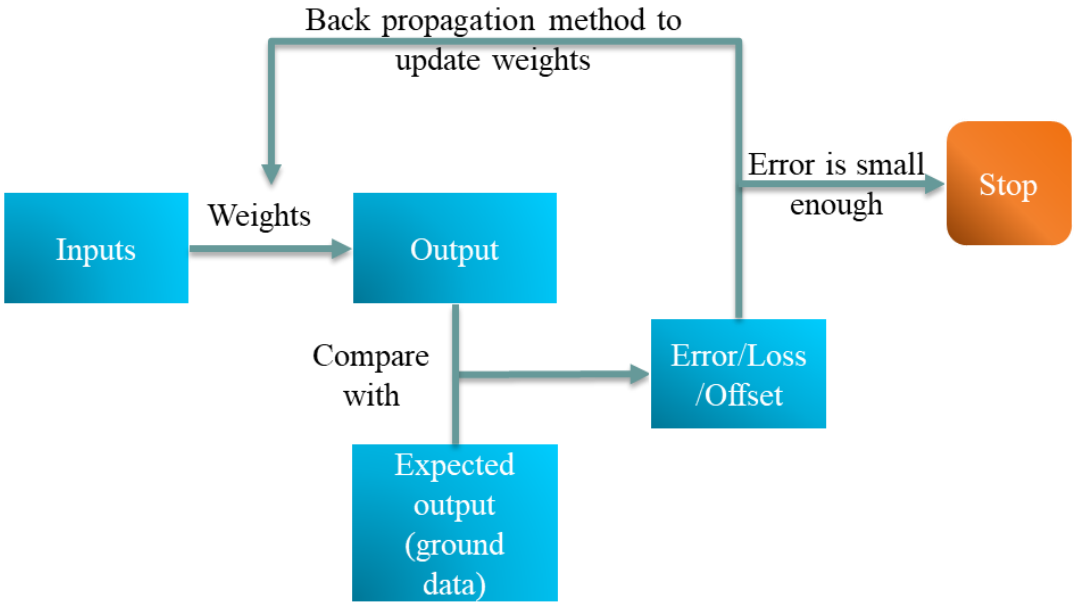

Figure 3. 1 Block diagram explaining neural network training algorithm

3.1.2 Activation functions

Activation function is a critical part of the neural network. It determines whether the output Y produced from the raw data inputted into the neural network is a

viable output. If the output falls within the range, then it is considered relatively accurate and is used in its predictions. Otherwise, it is rejected by the network, or "not activated." There are different activation functions that can be used to accomplish this goal, each having their own unique properties [70].

In this work, three different activation functions were used (Sigmoid, Tanh and ReLu). Mathematics format of the activation functions are described in the following paragraphs.

Table 3. 1 Activation function and corresponding mathematical expression

Activation function	Mathematical expression
Sigmoid	$A(x) = \frac{1}{1 + e^{-x}}$
Tanh	$A(x) = tanh(x) = \frac{2}{1 + e^{-2x}} - 1$
ReLu	$A(x) = max(0, x)$

Sigmoid functions are one of the most commonly used activation functions in neural network. It produces a smooth, nonlinear function that is bounded in range (0,1). Its gradient is steepest at the center and flattens out at both ends of the curve. Its nonlinear property allows the user to stack layers, it allows non-binary inputs as well. It also tends to become steeper towards the center of the model, meaning that the function will tend to assign Y values towards either end of the graph, making it

good at creating distinctions in its predictions. The biggest issue with the sigmoid function is that on either end of the graph, the gradient becomes increasingly small until it nearly disappears. This is an issue as at this point, the network's learning process slows down drastically until it seems that is has stopped altogether.

The tanh function is similar to the sigmoid function in both size and shape. It is nonlinear and has a smooth curve whose gradient flattens out at either of the end points. The only difference is the scaling is different, where unlike the sigmoid function, the tanh function has a range (-1,1). Due to this difference in scaling, the tanh curve has a much steeper gradient than the sigmoid curve. It also shares the issue of the decreasing gradient at both ends of the graph.

The ReLu is a nonlinear function only gives an output of x when x is positive, otherwise it outputs 0. It has a range [0, inf), which leads to an issue of not having a defined bound. This could lead to blowing up the activations as your data outputs are no longer within a bounded setting. A benefit for using ReLu is that it filters out any negative numbers produced, allowing the activations to be more efficient and the network to be lighter. However, because ReLu assigns negative numbers to output 0, it leads to the option that occasionally the gradient will go to 0. Once this happens, these points will no longer be affected by any changes in input and output, leading to inaccurate predictions.

3.1.3 Backpropagation method

Backpropagation method is normally used in ANN to determine the updates of weights [69]. The network produces a set of coefficients, or "weights", that is used to determine the amount of influence a certain input has in relation to the output. The

sum of these weights is passed through an activation function, which checks whether the calculated output is valid and can be used. In other words, the activation function determines whether connections made by the network can be "activated". With each iteration, the error is calculated between the predicted output and the actual output. The calculated error is used to make weight adjustments. The general steps of back propagation work in a following way. Firstly, a random weight to each input is assigned. Secondly, the weight is updated by the equation (10). Thirdly, updating will continue until the error reaches its lowest achievable value. The derivation of equation (10) is provided via the partial equations below (equation (1) to (10)).

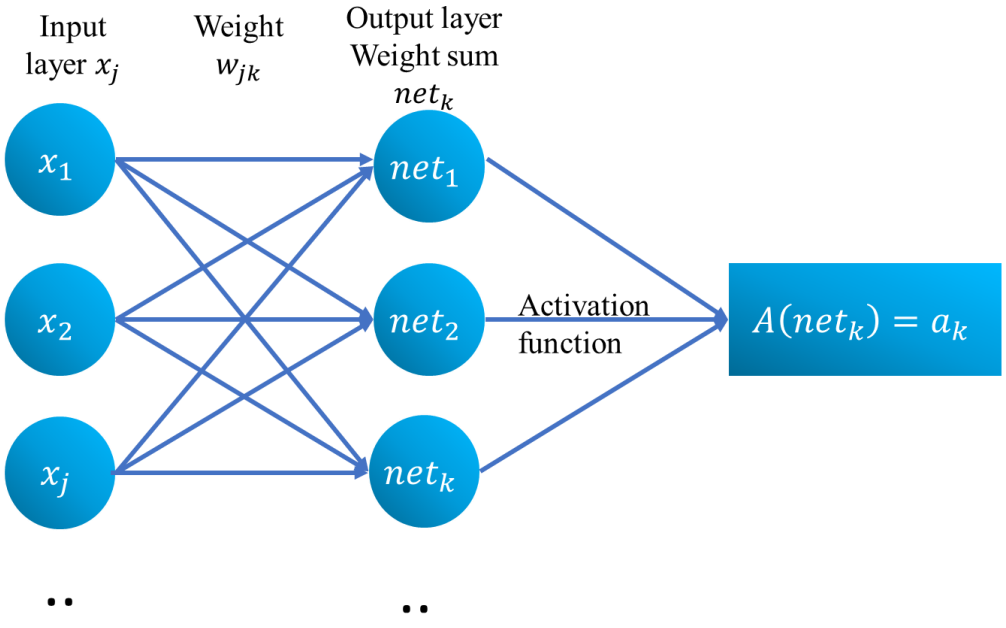

Figure 3. 2 Neural network model in this work

In this work, single layer neural network was used. Fig. 3.2 explains the notation of this explanation.

The subscript j denotes the input layer. The subscript k denotes the output layer. As mentioned before, the core idea of training of ANN in this study is by assigning an arbitrary number to the weight and updating and adjusting the weight. The adjustment of the weight follows the equation,

$$\Delta W \propto -\frac{\partial E}{\partial W} \quad (1)$$

where E(x) is called loss function and it is defined as,

$$E = \frac{1}{2}\sum_k (t_k - a_k)^2 \quad (2)$$

where t_k is the target value for output, a_k is the calculated output based on weight sum of inputs and activation function.

The weight change is then written as:

$$\Delta w_{jk} \propto -\frac{\partial E}{\partial w_{jk}} \quad (3)$$

It can be rewritten into,

$$\Delta w_{jk} = -\mathcal{E}\frac{\partial E}{\partial w_{jk}} \quad (4)$$

where $\mathcal{E}$ is an assigned constant. Here we call it as step distance.

Using chain rule, we can get that:

$$\Delta w_{jk} = -\mathcal{E}\frac{\partial E}{\partial a_k}\frac{\partial a_k}{\partial net_k}\frac{\partial net_k}{\partial w_{kj}} \quad (5)$$

Now let's take a look at the three partial derivatives respectively.

Substituting equation (2) into equation (5) we can get:

$$\frac{\partial E}{\partial a_k} = \frac{\partial(\frac{1}{2}(t_k - a_k)^2)}{\partial a_k} = -(t_k - a_k) \quad (6)$$

Activation function is used to normalize weight sum of inputs, and with that we can get:

$$\frac{\partial a_k}{\partial net_k} = \frac{dA(net_k)}{dnet_k} = A'(net_k) \quad (7)$$

A(x) is the activation function.

For example, if we use sigmoid as activation function, equation (7) will turn into:

$$\frac{\partial a_k}{\partial net_k} = \frac{dA(net_k)}{dnet_k} = A'(net_k) = a_k(1 - a_k) \quad (8)$$

Lastly,

$$\frac{\partial net_k}{\partial w_{kj}} = \frac{\partial (w_{kj} a_j)}{\partial w_{kj}} = a_j \quad (9)$$

where a_j is the output from the previous calculation.

With that, the weight update can be written into:

$$\Delta w_{kj} = \varepsilon(t_k - a_k)A'(net_k)a_j \quad (10)$$

Equation (10) is directly used in algorithm codes to update weights.

3.2 Experimental

In this work, algorithms were coded using python language. Source codes can be found in appendix. The data used to train the model are fitted impedance of overcharge and overdischarge from this research (included in appendix). Values of R1, R2, and R3 for each fitted cycle serve as input that are ultimately used to predict R1, R2, and R3 of future cycles (output). R1, R2, R3 represents ESR, R_{ct} and R_{sei}, respectively. The data of cycle 1 was used to predict the data of cycle 2, the data of cycle 2 is used to predict the data of cycle 3, and so on. The data is inputted in as an array containing the 3 elements. The training process is repeated over 50 million times of iterations. The accuracy of the predictions increases as the iterations the data was run through increases.

3.3 Results and discussions

Figure 3.3 shows the results of neural network prediction of R1 R2 and R3 using sigmoid method for normal charge and normal discharge data. (for the cycle 56^{th})

Percent error is defined as the following equation:

$$\text{Percent Error} = \frac{|experimental\ value - prediction\ value|}{experimental\ value} \times 100\%$$

As we can see from the results, the more times of training, the more accurate is the prediction. Specifically, the prediction of R1 and R3 does not change too much after first several iterations. In contrast, the prediction of R2 gradually changes with training time. All percent errors stabilize after around 50 million times of training. Besides, the percent error of R1 and R2 can be mostly minimized at 10% while R3 can be minimized at 15%.

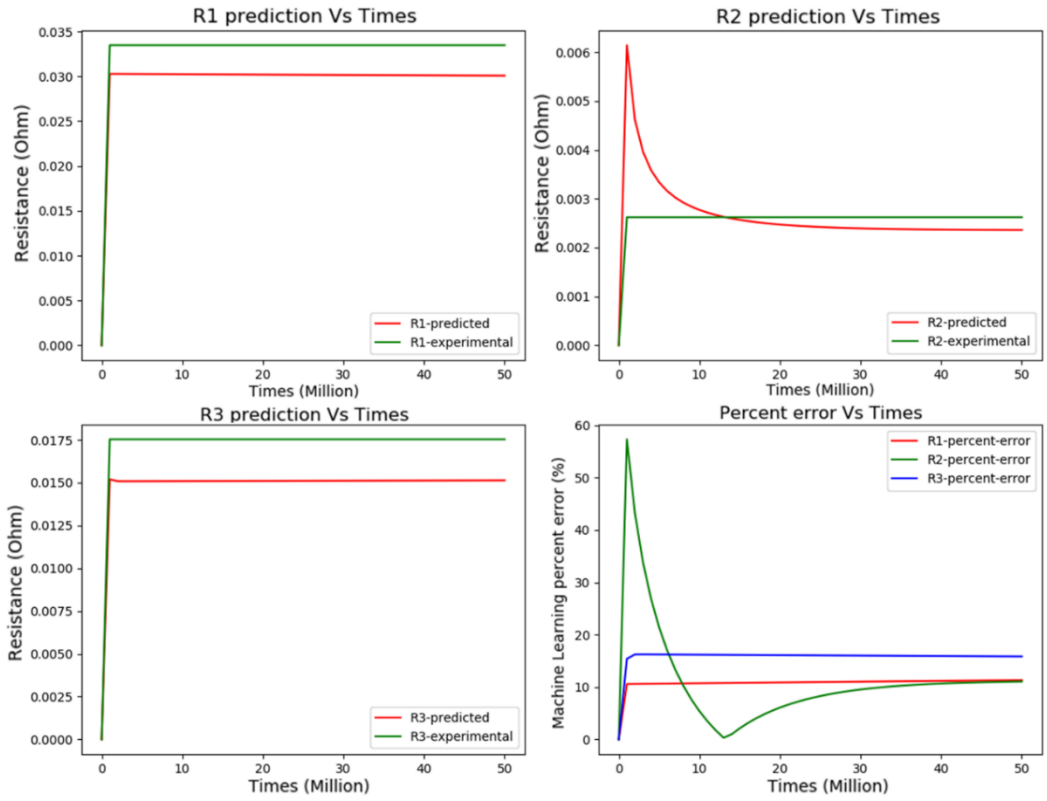

Figure 3. 3 Estimation results using Sigmoid as activation function (a) R1 (b) R2 (c) R3 prediction results and experiment results of 56th cycle normal charge and normal discharge and (d) percent error of three estimation in (a) (b) and (c) (x axis are iteration times that the model is trained)

Different activation functions were tried, and a better prediction was achieved using same group of data. Figure 3.4 shows the results of percent error using tanh and ReLu for normal charge and normal discharge at 56th cycles.

As we can see from the results, the percent error of tanh is 5%, 1.5% and 1% for R1, R2 and R3, respectively. The percent error curve using ReLu and Tanh are same under this case. The percent error of tanh method and ReLu is much smaller than Sigmoid. Overall, tanh and Relu give better predictions as in lower percent error than sigmoid. With that, we can draw a conclusion that different activation function

affects the predictions significantly.

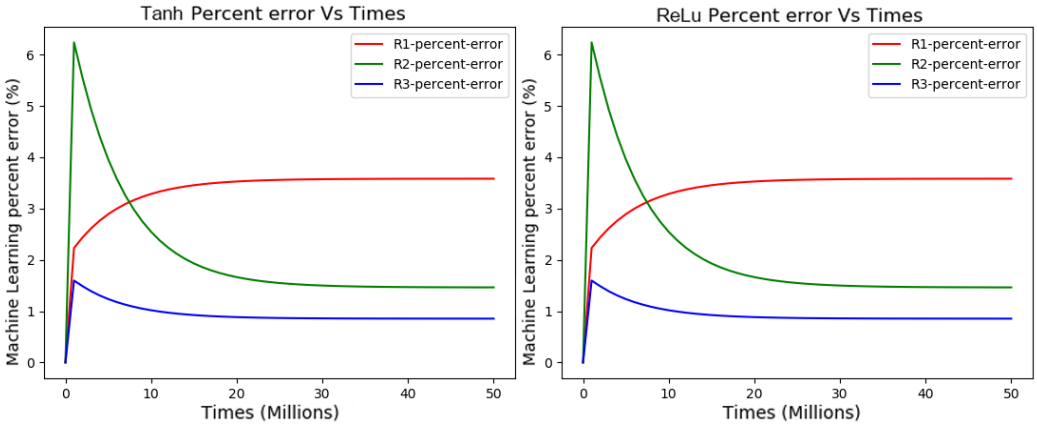

Figure 3. 4 Percent error using different activation function and same sets of data (a) percent error using Tanh activation function (b) percent error using ReLu as activation function for normal charge and normal discharge at 56th cycle

Lastly, all eight group of tests were run for the neural network training and a bigger percent error was found in some datasets. Figure 3.5 is a typical representative. Comparing Figure 3.5 with previous Sigmoid method, we can get the conclusion that with same activation function, the accuracy of prediction is also influenced by the input data.

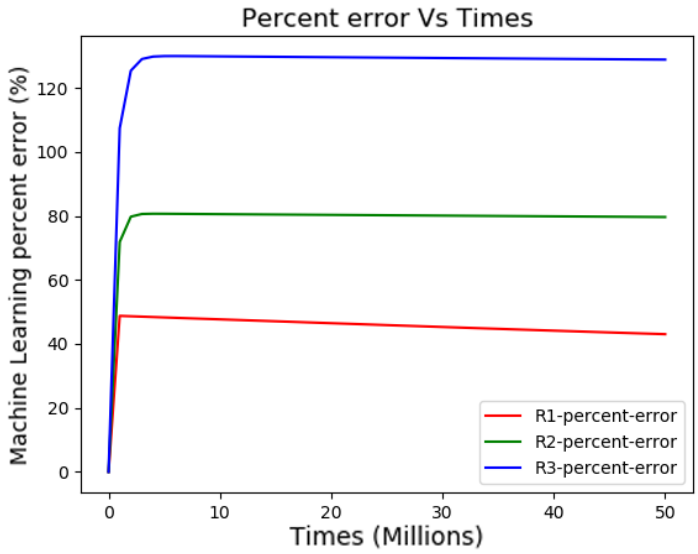

Figure 3. 5 Percent error of normal charge overdischarge cycle# using sigmoid as activation function

We propose that the followings are the factors that affect the accuracy of predictions using ANN for this experiment: 1. Choice of activation function; 2. Times of training; 3. Amount of training data; 4. Layers of neurons. For the first two factors, it has been proven from this work that they affect the accuracy of the prediction. The rest two factors (factor 3 and factor 4) are well known from previous work [69].

To help future development and improve the accuracy of the training, the following actions can be taken considering the factors above: 1) Gather more training data. Neural network prediction has a nature of the more data you put in, the more accuracy of percent error you get. Another way to improve the accuracy in future is to gather more training data of the battery. 2) Spend effort choosing a suitable activation function. Our results show that using different activation function will affect the results in a very dramatic way. Thus, a selection of different activation function for prediction will be a meaningful direction to look at for future researches. 3) Adding more layer of neurons. This work is a single layer of input and output with no hidden layers. If more data is provided, adding multiple layers will be able to improve the prediction and better imitating human thinking process.

Chapter 4

Embedded impedance analyze circuit within battery management systems

4.1 Basics of Battery Management Systems (BMS)

Battery Management System, by name, refers to that any electrical or mechanical systems which performs the function of managing battery cells or battery packs. Generally, a battery management system including the functions of monitoring, protecting, balancing and controlling of the battery. Fig. 4.1 [71] gives a more specific function list for battery management system.

		Reports individual cell voltages	Balances the battery	Requests that battery be switched off	Includes switch to turn off battery
Digital: knows where the problem is and by how much	Protector	✓	✓	✓	✓
	Balancer	✓	✓	✓	
	Monitor	✓		✓	
	Meter	✓			
Analog: knows there's a problem, but doesn't know where and by how much	Protector		✓	✓	✓
	Balancer		✓	✓	
	Monitor			✓	
	Regulator		✓		

Figure 4. 1 Battery Management System Function Table

BMS is always in the presence of a circuit broad. Here are some pictures of the battery management system [72], [73], see Fig. 4.2 and Fig. 4.3.

Figure 4. 2 Example of Battery Management System in Single Cell

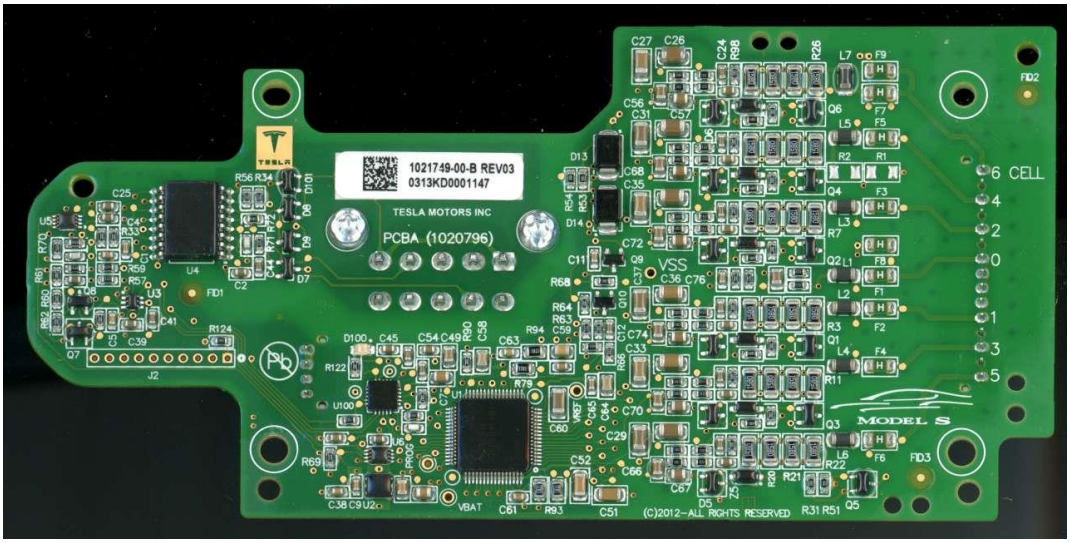

Figure 4. 3 Example of Battery Management System for Battery Module

4.2 Literature research of battery management systems (BMS)

Battery management system (BMS) doesn't have a strict definition. Basically, any system performs the function of managing the battery is supposed to be called battery management system. By field of study, BMS can be classified into electrical and mechanical part.

There are continuously works and researches on BMS through the years. Looking into researches on BMS, fours columns of studies focusing on four main functions of BMS is widely published. Which is State of Charge (SOC) estimation [74-77], State of Health (SOH) estimation [78-82], battery balancing and equalization [83] and thermal management [84 - 87]. Usually, battery Management System (BMS) varies from simple circuit chip to large systematic board based on the functions in need in different electronic devices applications. Generally speaking, a basic BMS performs functions of measurement, monitoring, protecting and balancing for the corresponding batteries. In the case of EV/HEV (Electric Vehicles/ Hybrid Electric Vehicles) BMS, in addition to performing the functions above, a successful BMS also requires a higher performance in monitoring and controlling of the state of health (SOH). This requires better understanding of SOH of the battery pack in use. Besides, battery pack management architecture design and power control is also needed for the successful performing of large battery packs.

The increasing demand for high mileage and safety in EV/HEVs, a BMS in real-time with more accuracy, more intelligence, more interactive and more functionality is necessary, which drives us to develop a new generation of smart BMS to fulfill the need.

4.3 Architecture and High-Level Design (Joint work)

Acknowledgment: this section is based on a joint work. Yige was collaborating with an undergrad senior design team: Jack Gu, Jack Gatfield and Joseph Gozum, and they were instructed by Dr. Roman Chomko. Writing contributed by undergrads has their name attached after the paragraph.

4.3.1 System Architecture and Design

HARDWARE:

Variable frequency Sine and Square wave generation: The variable frequency sine/square wave generation component is used primarily to power the current generation component of our project. The ability to easily switch frequencies with the desired range ($f \in [1\ Hz, 1\ KHz]$) serves a crucial part in our project as that is what allows us to achieve the goal of our project in the first place (Measuring impedance of the test battery at various frequencies). **(Jack Gu)**

Current generation and injection: The current injection is what we use to induce a response within the battery. It is this response that is picked up by the differential reading component of our circuit, allowing us to collect data on the impedance of the battery at the selected frequency. **(Jack Gu)**

Differential reading: Differential probes are placed in specific parts of the test circuit in order to measure the appropriate raw data for testing. In our case, we use the differential reading component to gather data on battery voltage as well as the value of the injected current via the voltage of a small load resistor in series. These voltage readings are then processed in order to obtain data. **(Jack Gu)**

Power distribution and voltage level division: Power is taken from a 12-volt DC power adapter and is then placed into the circuit. This provides a 12-volt line that powers the function chip and a line that we can manipulate to get the voltage levels the other components of the system require. A 5-volt voltage regulator was used to produce a 5-volt voltage line for the microcontroller, biasing circuitry, and digital potentiometer. A 10-volt regulator was used to produce a 10-volt voltage line for the differential amplifiers and the voltage inverter which was also used to power the op amp. This power was off course needed in order for the circuit to operate. **(Jack Gatfield)**

Microcontroller: The microcontroller is the primary data acquisition device. Its built-in 10-bit ADC is used to read the output of the differential op-amps and quantize it and it's USART capability is used to transmit the acquired data to the PC for further processing. **(Joseph Gozum)**

SOFTWARE:

Serial Communication: The microcontroller reads the ADC data and builds an array of the values. It then sends the array via USART to a terminal and is captured on the processing computer. **(Joseph Gozum)**

Data formatting: The data sent by the microcontroller and captured through the terminal cannot be understood correctly by MATLAB. We had to format the file using a python and a visual basic macro. The code converts that data into a voltage value that can used by MATLAB to determine the actual impedance. **(Jack Gatfield and Joseph Gozum)**

Cell Impedance Calculation: The rest of the system is meant to provide data for the MATLAB code to use to actually calculate the battery impedance. The code has to take out the nominal voltage of the battery, correct the data to account for the differential amplifier gains, and then it takes the data and averages the trials to reduce noise's influence on the results. Once the average voltage over the battery array and the current through the battery array is built the actual impedance calculations can begin. It first creates a sinusoidal approximation of the voltage array in order to calculate the phase shift the battery causes. Then after this calculation is performed it calculates the magnitude of the impedance and uses the phase shift to find the real and imaginary parts of the impedance. After all the calculations it outputs a graph of the data at the different frequencies for the user to see. **(Jack Gatfield)**

4.3.2 Hardware Architecture

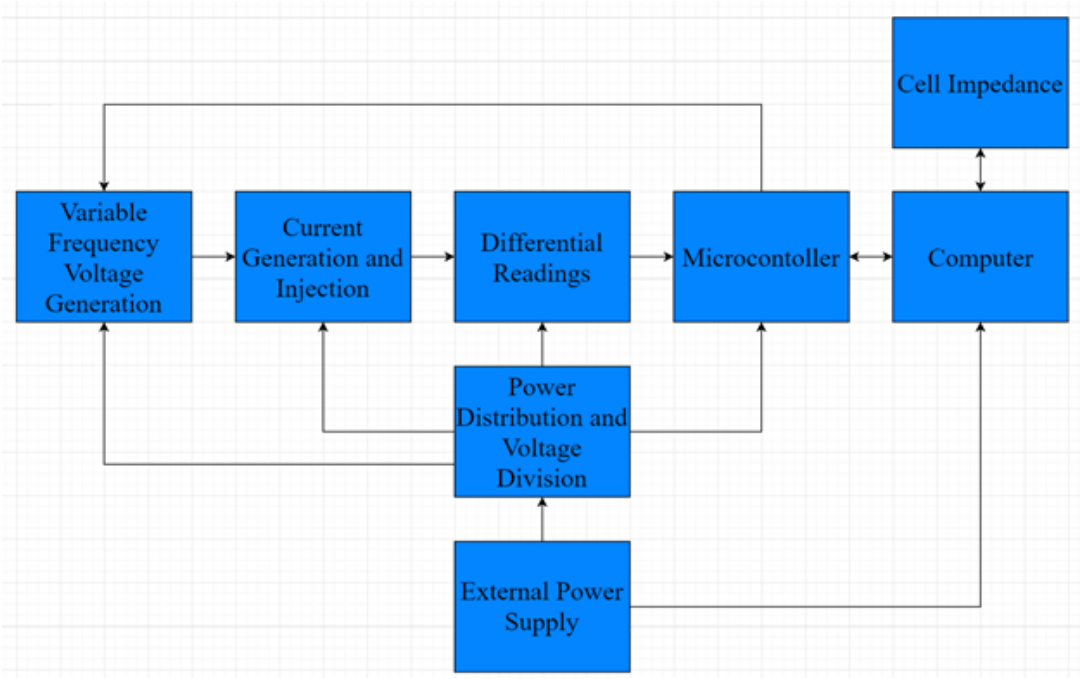

Figure 4. 4 Block diagram for project circuity

The hardware of this project consists of circuity, a microcontroller, and a computer. The circuity is meant to produce the data that is eventually collected and sent to the computer for processing. The microcontroller is meant to capture the analog data and transmit it to the computer while also taking user information from the computer and in turn setting the proper parameters in the circuity. The computer is meant to take the data and process it in order to obtain the wanted information but it also meant to take in user information and send it to the microcontroller to allow for the variables to be set. Above is a general block diagram of the system and below is a through board and PCB version of the circuit. **(Jack Gatfield)**

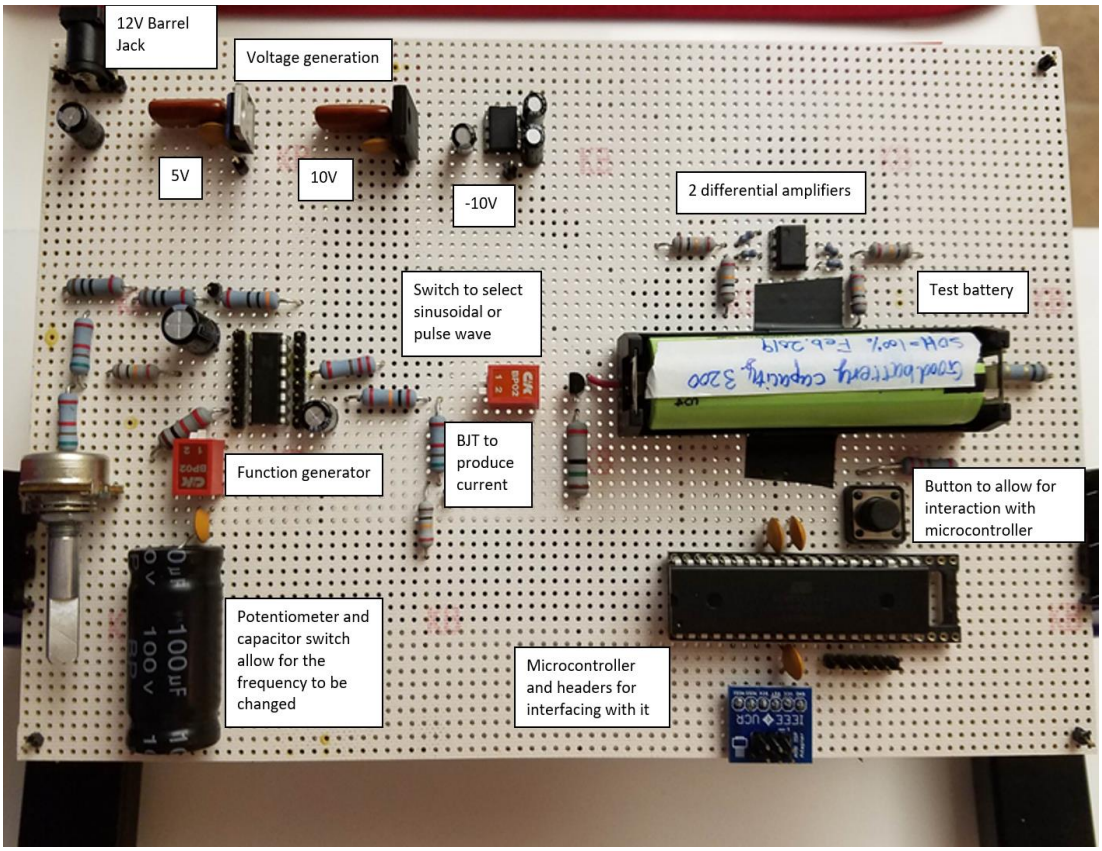

Figure 4. 5 Through Hole version of the circuity

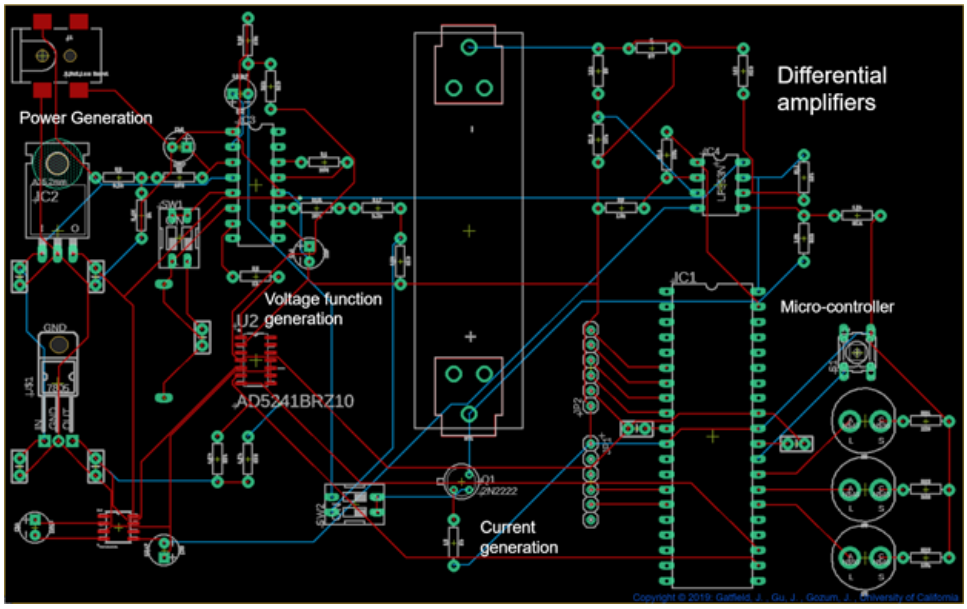

Figure 4. 6 PCB version of the circuity in Eagle PCB software

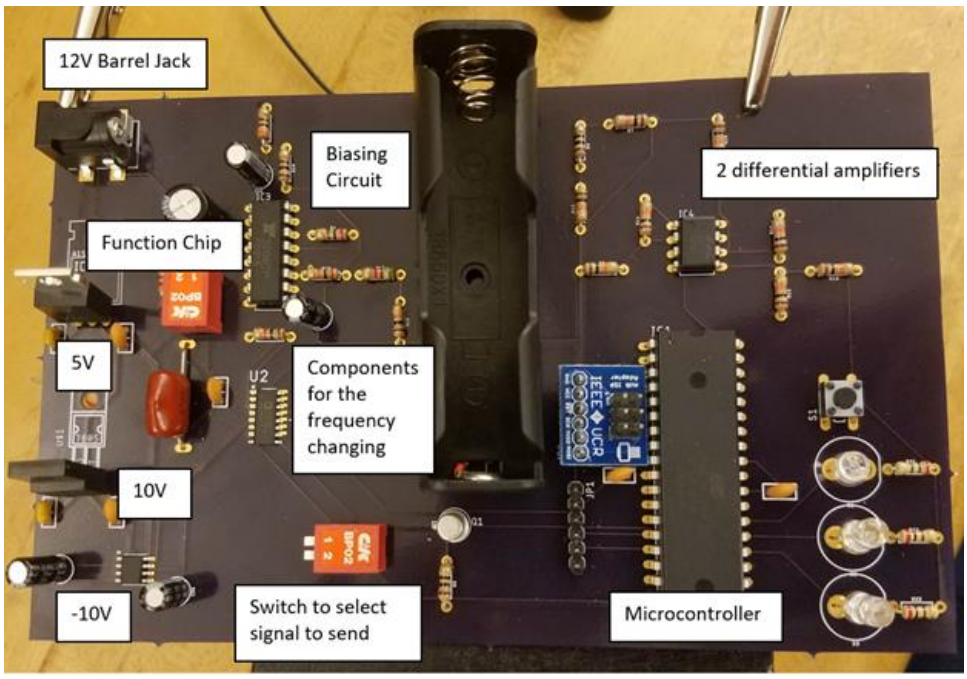

Figure 4. 7 PCB version of the circuity printed and assembled

Initially the plan was to go from the breadboard version of the circuit straight to the PCB version but due to several unexpected design changes the PCB version was forced to be pushed to a later date and made even later due to the printing time. To

compensate for this delay, the through hole version was developed to provide a clean and easy to view circuit that could be used for demonstration while also providing a solid circuit to stabilize data acquisition. **(Jack Gatfield)**

4.3.3 Software Architecture

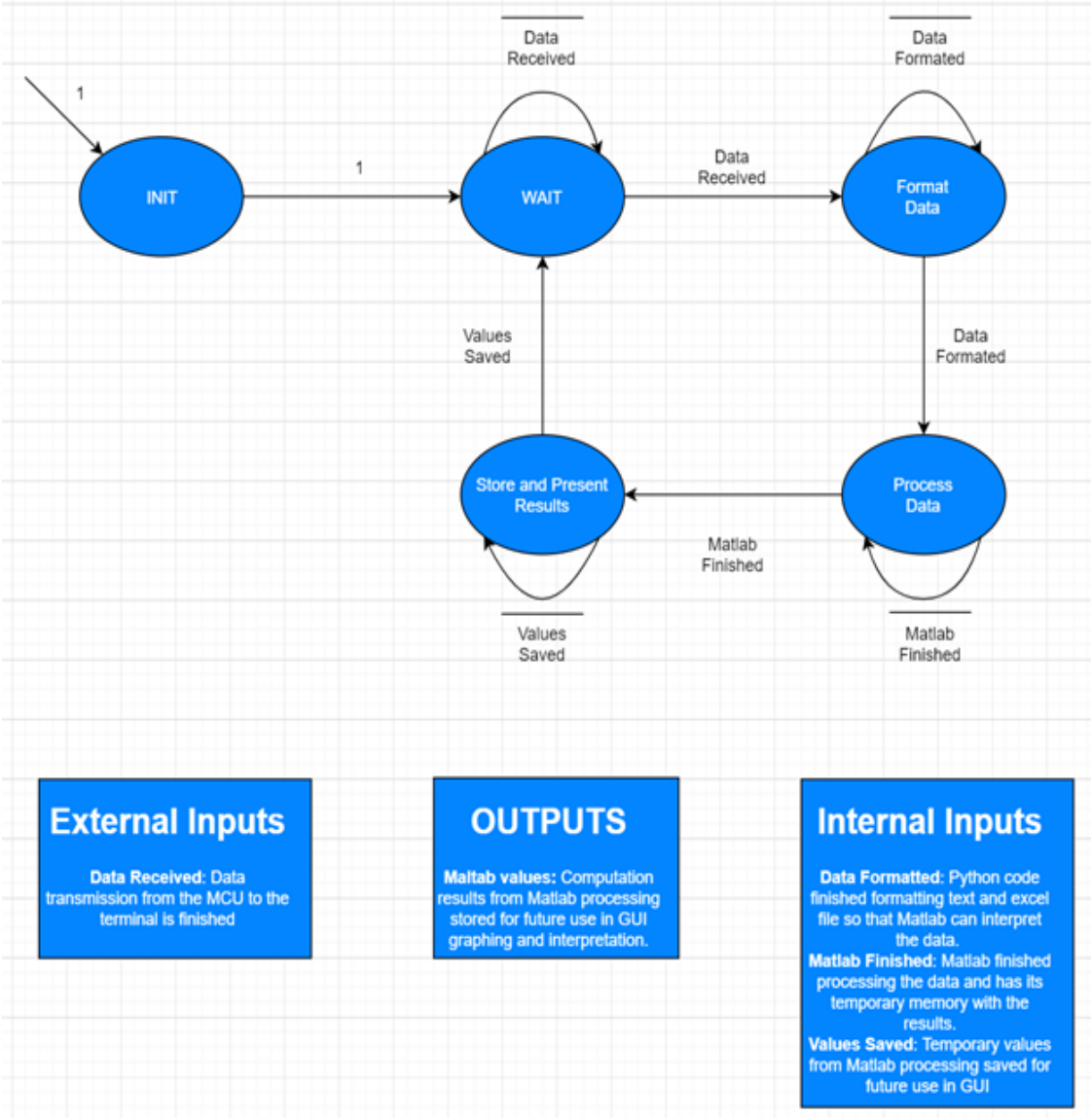

Figure 4. 8 State machine for computer processing

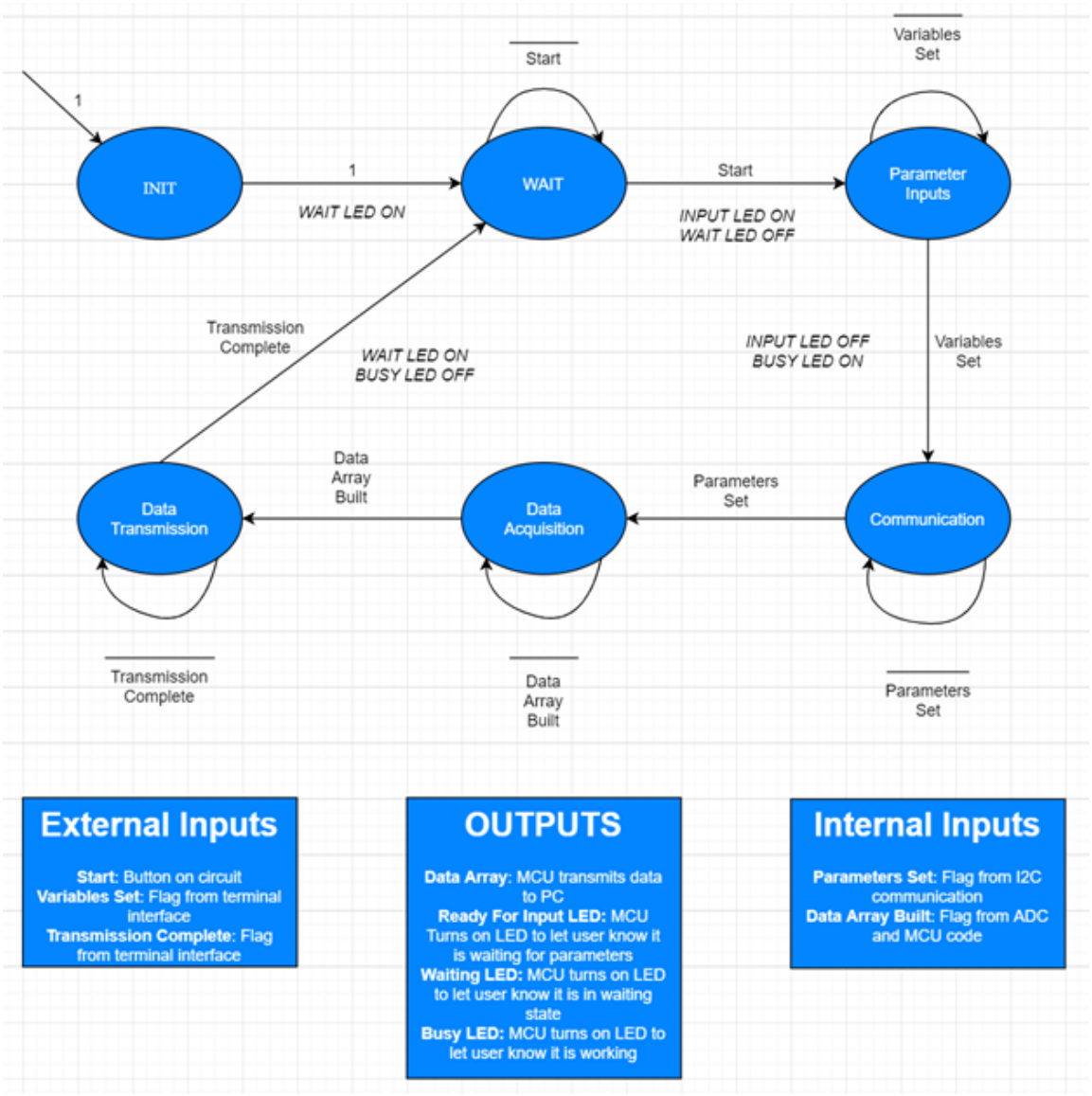

Figure 4. 9 State machine for microcontroller processing

For software our project used a microcontroller (Atmega1284P) and a computer. Figure 4.8 shows the state machine for the computer when processing the data. The computer is presented the data by the terminal, formats it so MATLAB can understand it, then processes it in order to obtain the needed values. It does this for the full frequency test range and then output the information in a figure. The

microcontroller has a much more complex state diagram shown in figure 4.9. The microcontroller has to communicate with the computer in order to transfer the data and take in the user specifications. It also has to communicate with the circuit elements (Digital potentiometers) to set the frequency of the function generator signal the user wants to test. On top of this it has to convert the data and store it. **(Jack Gatfield)**

4.3.4 Rationale and Alternatives

The reasoning for the hardware architecture is simply because it is the most direct approach that allows us to acquire the most pertinent data in order to calculate impedance. To consider other architectures or approaches would be unnecessary unless we are looking for some other functionality to include on the device. **(Joseph Gozum)**

A Finite-State Machine representation was chosen for the software architecture because our device is only in one specific state of operation at any given time and changes based on external inputs in a predefined sequence. A Finite-State Machine made a perfect fit for this type of device given how we intend for it to operate. This form of architecture is also not computationally intensive nor is it non-deterministic, this is perfect for implementation on the microcontroller utilized in our device which executes non-intensive commands sequentially. This architecture is also heavily event-driven which is required for our case because we need certain things to act based on certain external event/stimuli. Due to a lack of understanding

of different software architectures, no others were considered especially since a Finite-State Machine works perfectly fine for our use case. **(Joseph Gozum)**

The main rationale for our project was optimizing our system to be able to easy and efficient to implement while still getting accurate data effectively. For the hardware we took the most straightforward and efficient circuitry to allow for the data acquisition. For the software we took the path that was compatible on different operating systems and could still interact with the microcontroller. In the future a more complex system could be built using the design principles and implementation of our project. **(Jack Gatfield)**

Chapter 5

Conclusions

5.1 Conclusions and summaries

In summary, EIS analysis of NCR 18650B batteries were conducted to investigate the interactions among the internal components of the batteries.

First, the batteries were tested at different states of charges (SOC) under normal charging/discharging conditions. Then they were tested at fully charged states under different charging/discharging conditions with increased/lowered cut-off voltages. The values of equivalent series resistance (ESR), solid-electrolyte interphase layer resistance (R_{sei}) and charge-transfer resistance (R_{ct}) were determined from the EIS fitting using an equivalent circuit. For the batteries at different SOCs under normal charging/discharging conditions, there are fluctuations in R_{sei} and R_{ct} values during SOC sweeps because of the changes in the microstructure of the electrodes upon intercalation and deintercalation of lithium. However, the amplitude of those fluctuations are generally small and values of R_{sei} and R_{ct} does not change very much

since they depend strongly on the cycle number or aging of the batteries. For the batteries that were cycled longer with different cut-off voltages, ESR increases faster under overcharging, indicating a possible cobalt dissolution from the cathode. Furthermore, overcharging and overdischarging can cause the increase of R_{ct} due to the degradation of the interface between the electrode and the electrolyte. Besides, EIS fitting results of battery under different real-life usage scenarios are given.

In neural network modeling and prediction of battery SOH, ESR, R_{sei} and R_{ct} were used as the three indicators of comprehensive state of health (CSOH) of the batteries. Artificial neural network model was provided to predict the future values of these CSOH indicators by using the data from regular charging/discharging. By using ReLu or Tanh as the activation function percent errors of 5%, 1.5% and 1% for ESR, R_{sei} and R_{ct} were achieved, respectively. It was also seen that choice of the activation function will affect the accuracy of prediction. Although this work has a single layer of input and output with no hidden layers in the provided neural network model, it still provides acceptably accurate predictions. In order to improve the accuracy of the prediction, more data with multiple layers need to be introduced to the model. The training algorithm and the results of this work can be used as a simple and effective approach to help researchers develop new models for comprehensive state of health prediction of lithium ion batteries.

Lastly, a design of impedance analysis circuit is given which make it possible to conduct real time impedance measurement on battery management systems (BMS).

5.2 Contributions

In this work, three main tasks were achieved:

1) In-depth understanding battery degradation mechanism under different cycling conditions through the analysis of side reactions was achieved;
2) Innovative design of new functionality of BMS to enable battery safety warning and real time SOH diagnoses on board;
3) Neural network training algorithm that preform accurate battery comprehensive SOH estimation and prediction.

This work has two main contributions to the field of research:

1) EIS studies helps researchers better understand aging mechanism of commercial lithium ion battery, this might help them with other battery analysis using different characterization methods such as CV, GITT, XRD, SEM etc;
2) The neural network training algorithm from this work can be also used as a simple and efficient model to aid researchers to validate their electrochemical analysis.

This work has three main contributions to the field of industry:

1) EIS studies helps the industry better understanding aging mechanism of commercial lithium ion battery, this might help them with updating battery cycling protocol to improve battery efficiency and lifetime in any NCA battery applications.
2) The Innovative design of new functionality of BMS to enable battery safety warning and real time SOH diagnoses on board, this helps to improve the

safety in electric vehicles, energy storage systems, and electricity grid;

3) Neural network training algorithm that preform accurate battery comprehensive SOH estimation and prediction, this can be used for battery life span estimation for battery maintenance and price per year calculation.

Bibliography

[1] BP (2016). BP Statistical Review of World Energy 2016 http://www.bp.com/content/dam/bp/pdf/energy-economics/statistical-review-2016/bp-statistical-review-of-world-energy-2016-full-report.pdf

[2] Effects of global warming https://www.nationalgeographic.com/environment/global-warming/global-warming-effects/

[3] 5 Key Threats to California From Climate Change https://news.nationalgeographic.com/news/2014/08/140812-california-climate-change-global-warming-science/

[4] IPCC (2014) https://www.ipcc.ch/report/ar5/wg3/

[5] The Union of Concerned Scientists https://www.ucsusa.org/global-warming#.WxN8Nkgvy00

[6] What Changed In The Electric Vehicle Industry In Quarter 1, 2018? https://cleantechnica.com/2018/04/05/what-changed-in-the-electric-vehicle-industry-in-quarter-1-2018/

[7] Dynamics in the global electric-vehicle market https://www.mckinsey.com/industries/automotive-and-assembly/our-insights/dynamics-in-the-global-electric-vehicle-market

[8] Tarascon J.-M., Armand M., Issues and challenges facing rechargeable lithium batteries. Nature 414, 359–367 (2001).

[9] Goodenough J. B., Kim Y., Challenges for rechargeable Li batteries. Chem. Mater. 22, 587–603 (2010).

[10] Armand M., Tarascon J.-M., Building better batteries. Nature 451, 652–657 (2008).

[11] Choi J. W., Aurbach D., Promise and reality of post-lithium-ion batteries with high energy densities. Nat. Rev. Mater. 1, 16013 (2016).

[12] Zerrin, T., Ozkan, M., & Ozkan, C. (2018). Improved electrochemical performance of LiCoO2 electrodes for high-voltage operations by Ag thin film coating via magnetron sputtering. *MRS Advances, 3*(60), 3513-3518.

doi:10.1557/adv.2018.517

[13] M. Berecibar, I. Gandiaga, I. Villarreal, N. Omar, J. Van Mierlo, and P. Van Den Bossche, “Critical review of state of health estimation methods of Li-ion batteries for real applications,” vol. 56, pp. 572–587, 2016.

[14] Y. Zou, X. Hu, H. Ma, and S. E. Li, “Combined State of Charge and State of Health estimation over lithium-ion battery cell cycle lifespan for electric vehicles,” J. Power Sources, vol. 273, pp. 793–803, 2015.

[15]. Z.M. Salameh, M.A. Casacca, W.A. Lynch, IEEE Trans. Energy Convers. 7 (1992) 93-98.

[16]. M. Chen, G. Rin_con-Mora, IEEE Trans. Energy Convers. (2006) 504-511.

[17] I.S. Kim, IEEE Trans. Power Electron. 23 (2008) 2027-2034.

[18] A. Nuhic, T. Terzimehic, T. Soczka-Guth, M. Buchholz, and K. Dietmayer, “Health diagnosis and remaining useful life prognostics of lithium-ion batteries using data-driven methods,” J. Power Sources, vol. 239, pp. 680–688, 2013.

[19] A. Eddahech, O. Briat, N. Bertrand, J. Y. Delétage, and J. M. Vinassa, “Behavior and state-of-health monitoring of Li-ion batteries using impedance spectroscopy and recurrent neural networks,” Int. J. Electr. Power Energy Syst., vol. 42, no. 1, pp. 487–494, 2012.

[20] J. Remmlinger, M. Buchholz, M. Meiler, P. Bernreuter, and K. Dietmayer, “State-of-health monitoring of lithium-ion batteries in electric vehicles by on-board

[21] M. Dalal, J. Ma, and D. He, “Lithium-ion battery life prognostic health management system using particle filtering framework,” Proc. Inst. Mech. Eng. Part O J. Risk Reliab., vol. 225, no. 1, pp. 81–90, 2011.

[22] X. Lin et al., “Online parameterization of lumped thermal dynamics in cylindrical lithium ion batteries for core temperature estimation and health monitoring,” IEEE Trans. Control Syst. Technol., vol. 21, no. 5, pp. 1745–1755, 2013.

[23] T. Hansen, C.J. Wang, J. Power Sources 141 (2005) 351-358.

[24] S. Malkhandi, Eng. Appl. Artif. Intell. 19 (2006) 479-485.

[25] W.X. Shen, Energy Convers. Manag. 48 (2007) 433-442.

[26] L. Xu, J. Wang, Q. Chen, Energy Convers. Manag. 53 (2012) 33-39.

internal resistance estimation,” vol. 196, pp. 5357–5363, 2011.

[27] G. L. Plett, “Extended Kalman filtering for battery management systems of LiPB-based HEV battery packs - Part 3. State and parameter estimation,” J. Power Sources, vol. 134, no. 2, pp. 277–292, 2004.

[28] P. Singh, R. Vinjamuri, X. Wang, and D. Reisner, “Fuzzy logic modeling of EIS measurements on lithium-ion batteries,” Electrochim. Acta, vol. 51, no. 8–9, pp. 1673–1679, 2006.

[29] G. K. Prasad and C. D. Rahn, “Model based identification of aging parameters

in lithium ion batteries," J. Power Sources, vol. 232, pp. 79–85, 2013.

[30] S. A. Kalogirou, "Artificial neural networks in renewable energy systems applications: A review," Renew. Sustain. Energy Rev., vol. 5, no. 4, pp. 373–401, 2000.

[31] A. M. Darcy, A. K. Louie, and L. W. Roberts, "Machine learning and the profession of medicine," JAMA - J. Am. Med. Assoc., vol. 315, no. 6, pp. 551–552, 2016.

[32] M. Tkáč and R. Verner, "Artificial neural networks in business: Two decades of research," Appl. Soft Comput. J., vol. 38, pp. 788–804, 2016.

[33] Orazem, Mark E., and Bernard Tribollet. Electrochemical impedance spectroscopy. John Wiley & Sons, 2017.

[34] Lasia, Andrzej. "Electrochemical impedance spectroscopy and its applications." *Modern aspects of* electrochemistry. Springer, Boston, MA, 2002. 143-248.

[35] Jorcin, Jean-Baptiste, et al. "CPE analysis by local electrochemical impedance spectroscopy." Electrochimica Acta 51.8-9 (2006): 1473-1479.

[36] B. V. Ratnakumar, M. C. Smart and S. Surampudi, "Electrochemical impedance spectroscopy and its applications to lithium ion cells," Seventeenth Annual Battery Conference on Applications and Advances. Proceedings of Conference (Cat. No.02TH8576), Long Beach, CA, USA, 2002, pp. 273-277.

[37] M. Grossi, G. D. Lecce, T. G. Toschi and B. Riccò, "Fast and Accurate Determination of Olive Oil Acidity by Electrochemical Impedance Spectroscopy," in IEEE Sensors Journal, vol. 14, no. 9, pp. 2947-2954, Sept. 2014.

[38] G.S. Popkirov, Fast time-resolved electrochemical impedance spectroscopy for investigations under nonstationary conditions, Electrochimica Acta, Volume 41, Issues 7–8, 1996, Pages 1023-1027, ISSN 0013-4686.

[39] J. B. Goodenough and K. S. Park, "The Li-ion rechargeable battery: A perspective," J. Am. Chem. Soc., vol. 135, no. 4, pp. 1167–1176, 2013.

[40] Choi, H. C.; Jung, Y. M.; Noda, I.; Kim, S. B. (2003). "A Study of the Mechanism of the Electrochemical Reaction of Lithium with CoO by Two-Dimensional Soft X-ray Absorption Spectroscopy (2D XAS), 2D Raman, and 2D Heterospectral XAS−Raman Correlation Analysis". The Journal of Physical Chemistry B. 107 (24): 5806–5811. doi:10.1021/jp030438w.

[41] Amatucci, G. G. (1996). "CoO2, the End Member of the Li xCoO2 Solid Solution". Journal of the Electrochemical Society. 143 (3): 1114–1123. doi:10.1149/1.1836594.

[42] A. K. Hjelm and G. Lindbergh, "Experimental and theoretical analysis of LiMn2O4 cathodes for use in rechargeable lithium batteries by electrochemical impedance spectroscopy (EIS)," Electrochim. Acta, vol. 47, no. 11, pp. 1747–1759, 2002.

[43] J. B. Jorcin, M. E. Orazem, N. Pébère, and B. Tribollet, “CPE analysis by local electrochemical impedance spectroscopy,” Electrochim. Acta, vol. 51, no. 8–9, pp. 1473–1479, 2006.

[44] D. Dees, E. Gunen, D. Abraham, A. Jansen, and J. Prakash, “Electrochemical Modeling of Lithium-Ion Positive Electrodes during Hybrid Pulse Power Characterization Tests,” J. Electrochem. Soc., vol. 155, no. 8, p. A603, 2008.

[45] J. Guo, A. Sun, X. Chen, C. Wang, and A. Manivannan, “Cyclability study of silicon-carbon composite anodes for lithium-ion batteries using electrochemical impedance spectroscopy,” Electrochim. Acta, vol. 56, no. 11, pp. 3981–3987, 2011.

[46] Z. Deng, Z. Zhang, Y. Lai, J. Liu, J. Li, and Y. Liu, “Electrochemical Impedance Spectroscopy Study of a Lithium/Sulfur Battery: Modeling and Analysis of Capacity Fading,” J. Electrochem. Soc., vol. 160, no. 4, pp. A553–A558, 2013.

[47] S. EROL, “Electrochemical Impedance Spectroscopy Analysis and Modeling of Lithium Cobalt Oxide/Carbon Batteries,” Univ. Florida, 2015.

[48] D. Andre, M. Meiler, K. Steiner, H. Walz, T. SOCzka-Guth, and D. U. Sauer, “Characterization of high-power lithium-ion batteries by electrochemical impedance spectroscopy. II: Modelling,” J. Power Sources, vol. 196, no. 12, pp. 5349–5356, 2011.

[49] M. Drahansky et al., “We are IntechOpen , the world ’ s leading publisher of Open Access books Built by scientists , for scientists TOP 1 %,” Intech, vol. i, no. tourism, p. 13, 2016.

[50] G. Ning, B. Haran, and B. N. Popov, “Capacity fade study of lithium-ion batteries cycled at high discharge rates,” J. Power Sources, vol. 117, no. 1–2, pp. 160–169, 2003.

[51] U. Tröltzsch, O. Kanoun, and H. R. Tränkler, “Characterizing aging effects of lithium ion batteries by impedance spectroscopy,” Electrochim. Acta, vol. 51, no. 8–9, pp. 1664–1672, 2006.

[52] B. Campbell et al., “Carbon-Coated, Diatomite-Derived Nanosilicon as a High Rate Capable Li-ion Battery Anode.,” Sci. Rep., vol. 6, no. October, p. 33050, 2016.

[53] Illig, Jörg, et al. "Separation of charge transfer and contact resistance in LiFePO4-cathodes by impedance modeling." Journal of The Electrochemical Society 159.7 (2012): A952-A960.

[54] F. Gao and Z. Tang, “Kinetic behavior of LiFePO4/C cathode material for lithium-ion batteries,” Electrochim. Acta, vol. 53, no. 15, pp. 5071–5075, 2008.

[55] C. Betzin and H. Wolfschmidt, “Ageing Behavior of LiNi_{0.80} Co_{0.15}Al_{0.05}O₂ Cathode Based Lithium Ion Cells—Influence of Phase Transition Processes,” Mater. Sci. Appl., vol. 09, no. 01, pp. 155–173, 2018.

[56] S. S. Zhang, K. Xu, and T. R. Jow, “EIS study on the formation of solid electrolyte interface in Li-ion battery,” Electrochim. Acta, vol. 51, no. 8–9, pp. 1636–

1640, 2006.

[57] S. S. Zhang, K. Xu, and T. R. Jow, “EIS study on the formation of solid electrolyte interface in Li-ion battery,” Electrochim. Acta, vol. 51, no. 8–9, pp. 1636–1640, 2006.

[58] M. Itagaki, S. Yotsuda, N. Kobari, K. Watanabe, S. Kinoshita, and M. Ue, “Electrochemical impedance of electrolyte/electrode interfaces of lithium-ion rechargeable batteries: Effects of additives to the electrolyte on negative electrode,” Electrochim. Acta, vol. 51, no. 8–9, pp. 1629–1635, 2006.

[59] Barsoukov, Evgenij, and J. Ross Macdonald, eds. Impedance spectroscopy: theory, experiment, and applications. John Wiley & Sons, 2018.

[60] Dong, B., Ahmed, K., Li, Y., Ozkan, C. S., & Ozkan, M. (2017). Characterization of Thermal Behavior of Commercial NCR 18650B Batteries under Varying Cycling Conditions. MRS Advances, 2(54), 3329-3334.

[61] Dong, B., Li, Y., Ahmed, K., Ozkan, C. S., & Ozkan, M. (2018). Adoption of thermal behavior as an indicator for enhancement of the EIS analysis for NCR 18650B Commercial Lithium-ion batteries system. MRS Advances, 3(53), 3155-3162.

[62] Ahmed, K., Bell, J., Ye, R., Dong, B., Li, Y., Ozkan, C. S., & Ozkan, M. (2017). A Study of Diffusion in Lithium-ion Electrodes Under Fast Charging Using Electrochemical Impedance Spectroscopy. MRS Advances, 2(54), 3309-3315.

[63] C. R. Fell, D. Qian, K. J. Carroll, M. Chi, J. L. Jones, and Y. S. Meng, “Correlation between oxygen vacancy, microstrain, and cation distribution in lithium-excess layered oxides during the first electrochemical cycle,” Chem. Mater., vol. 25, no. 9, pp. 1621–1629, 2013.

[64] C. Li et al., “Towards flexible binderless anodes: silicon/carbon fabrics via double-nozzle electrospinning,” Chem. Commun., vol. 52, pp. 11398 – 11401, 2016.

[65] M. B. Pinson and M. Z. Bazant, “Theory of SEI Formation in Rechargeable Batteries: Capacity Fade, Accelerated Aging and Lifetime Prediction,” pp. 1–29.

[66] D. Dees, E. Gunen, D. Abraham, A. Jansen, and J. Prakash, “Electrochemical Modeling of Lithium-Ion Positive Electrodes during Hybrid Pulse Power Characterization Tests,” J. Electrochem. Soc., vol. 155, no. 8, p. A603, 2008.

[67] D. R. Franceschetti and J. R. Macdonald, “Electrochemistry 563,” Electrochemistry, pp. 563 – 567.

[68] Z. B. Stoynov, D. E. Vladikova, and B. Academy, “Basics of Electrochemical Impedance Spectroscopy,” no. 1, pp. 632 – 642, 2009.

[69] https://skymind.ai/wiki/neural-network

[70] https://ml-cheatsheet.readthedocs.io/en/latest/activation_functions.html

[71] Elithion Battery Management System
http://elithion.com/battery_management_systems.php

[72] Lithium-ion battery monitoring electronics (over-charge and deep-discharge protection) https://en.wikipedia.org/wiki/Lithium-ion_battery

[73] Tesla battery management system for battery module https://teslamotorsclub.com/tmc/threads/pics-info-inside-the-battery-pack.34934/

[74] H. He, R. Xiong, and J. Fan, "Evaluation of lithium-ion battery equivalent circuit models for state of charge estimation by an experimental approach," Energies, vol. 4, no. 4, pp. 582–598, 2011.

[75] H. He, X. Zhang, R. Xiong, Y. Xu, and H. Guo, "Online model-based estimation of state-of-charge and open-circuit voltage of lithium-ion batteries in electric vehicles," Energy, vol. 39, no. 1, pp. 310–318, 2012.

[76] S. Lee, J. Kim, J. Lee, and B. H. Cho, "State-of-charge and capacity estimation of lithium-ion battery using a new open-circuit voltage versus state-of-charge," J. Power Sources, vol. 185, no. 2, pp. 1367–1373, 2008.

[77] F. Sun, X. Hu, Y. Zou, and S. Li, "Adaptive unscented Kalman filtering for state of charge estimation of a lithium-ion battery for electric vehicles," Energy, vol. 36, no. 5, pp. 3531–3540, 2011.

[78] M. Dalal, J. Ma, and D. He, "Lithium-ion battery life prognostic health management system using particle filtering framework," Proc. Inst. Mech. Eng. Part O J. Risk Reliab., vol. 225, no. 1, pp. 81–90, 2011.

[79] A. Eddahech, O. Briat, N. Bertrand, J. Y. Delétage, and J. M. Vinassa, "Behavior and state-of-health monitoring of Li-ion batteries using impedance spectroscopy and recurrent neural networks," Int. J. Electr. Power Energy Syst., vol. 42, no. 1, pp. 487–494, 2012.

[80] X. Lin et al., "Online parameterization of lumped thermal dynamics in cylindrical lithium ion batteries for core temperature estimation and health monitoring," IEEE Trans. Control Syst. Technol., vol. 21, no. 5, pp. 1745–1755, 2013.

[81] A. Nuhic, T. Terzimehic, T. Soczka-Guth, M. Buchholz, and K. Dietmayer, "Health diagnosis and remaining useful life prognostics of lithium-ion batteries using data-driven methods," J. Power Sources, vol. 239, pp. 680–688, 2013.

[82] J. Remmlinger, M. Buchholz, M. Meiler, P. Bernreuter, and K. Dietmayer, "State-of-health monitoring of lithium-ion batteries in electric vehicles by on-board internal resistance estimation," vol. 196, pp. 5357–5363, 2011.

[83] S. W. Moore and P. J. Schneider, "A Review of Cell Equalization Methods for Lithium Ion and Lithium Polymer Battery Systems," no. 724, 2001.

[84] S. Al-Hallaj and J. R. Selman, "Thermal modeling of secondary lithium batteries for electric vehicle/hybrid electric vehicle applications," J. Power Sources, vol. 110, no. 2, pp. 341–348, 2002.

[85] S. Al Hallaj, H. Maleki, J. S. Hong, and J. R. Selman, "Thermal modeling and design considerations of lithium-ion batteries," pp. 1–8, 1999.

[86] G. Karimi and X. Li, “Thermal management of lithium-ion batteries for electric vehicles,” no. January 2012, pp. 13–24, 2013.

[87] S. A. Khateeb, S. Amiruddin, M. Farid, J. R. Selman, and S. Al-hallaj, “Thermal management of Li-ion battery with phase change material for electric scooters : experimental validation,” vol. 142, pp. 345 – 353, 2005.

Appendix

Appendix A. EIS fitted data (Ground data) used in neural network modeling

Table a. 1 Raw data of equivalent circuit fitted results for four group of tests

Normal Charge Normal Discharge								
cycle #	L1 (H)	R1 (Ohm)	Q1 (F.s^(a - 1))	R2 (Ohm)	Q2 (F.s^(a - 1))	R3 (Ohm)	Q3 (F.s^(a - 1))	Q4 (F.s^(a - 1))
1	4.64E-07	0.03412	6.51551	0.00268	1.64896	0.01598	936.1857	869.8691
10	4.75E-07	0.03193	1.401	0.00268	4.28749	0.01523	1842.979	1064.335
19	4.80E-07	0.0316	3.94695	0.00268	4.24895	0.01547	1864.113	1082.873
28	4.83E-07	0.03176	1253.81	0.00269	4.24287	0.0165	1886.104	1101.21
37	4.83E-07	0.03197	2534.758	0.00264	4.22326	0.01646	1941.523	1149.944
46	4.82E-07	0.03224	1257.847	0.00263	4.1843	0.01713	1952.941	1159.023
55	4.80E-07	0.03226	1126.93	0.00262	4.16843	0.01754	1961.392	1165.467
64	4.74E-07	0.03347	271.699	0.00262	4.16834	0.01753	1963.05	1166.784

Normal Charge Overdischarge								
cycle #	L1 (H)	R1 (Ohm)	Q2 (F.s^(a - 1))	R2 (Ohm)	Q3 (F.s^(a - 1))	R3 (Ohm)	Q4 (F.s^(a - 1))	Q5 (F.s^(a - 1))
1	4.77E-07	0.03308	0.08589	0.00465	2.10084	0.01201	451.9195	2.45E+21
10	5.21E-07	0.0304	0.00504	0.00557	2.11686	0.01256	457.8241	2.45E+21
19	5.09E-07	0.03207	0.01101	0.00553	2.15878	0.01321	459.4898	2.45E+21
28	4.95E-07	0.03082	0.00173	0.00548	2.16494	0.01267	470.5727	2.45E+21
37	5.18E-07	0.03303	0.00533	0.00548	2.16696	0.01276	471.4635	2.45E+21
46	5.13E-07	0.0336	0.00451	0.00549	2.18257	0.01309	474.2017	2.45E+21
55	5.11E-07	0.03405	0.00688	0.00549	2.18955	0.01326	475.0127	2.45E+21
64	4.94E-07	0.03522	0.01265	0.00551	2.20235	0.01365	476.916	2.45E+21
73	4.97E-07	0.03545	0.00873	0.00552	2.2735	0.01502	486.1134	2.45E+21
82	4.95E-07	0.0365	0.01458	0.00554	2.28941	0.01548	489.093	2.45E+21
91	4.71E-07	0.03826	0.01981	0.00546	2.34427	0.01581	501.4659	2.45E+21

Overcharge Normal Discharge								
cycle #	L1 (H)	R1 (Ohm)	Q1 (F.s^(a - 1))	R2 (Ohm)	Q2 (F.s^(a - 1))	R3 (Ohm)	Q3 (F.s^(a - 1))	Q4 (F.s^(a - 1))
1	4.30E-07	0.03282	0.43458	0.01055	5.47752	0.01239	377.5634	1.75E+07
10	4.32E-07	0.03409	0.49911	0.0094	6.4607	0.02118	344.9509	1.41E+17
19	4.36E-07	0.03467	0.54279	0.00796	6.77392	0.02121	210.3087	9722.858
28	4.39E-07	0.03549	0.96153	0.00796	8.21065	0.01998	191.8766	3712.63
37	4.36E-07	0.03705	0.71108	0.00801	8.60637	0.02511	196.3077	13187.54
46	4.36E-07	0.03814	0.6211	0.00798	8.96716	0.02754	178.6775	2.38E+91
55	4.38E-07	0.03894	0.64798	0.00777	9.2474	0.02802	174.6451	579893.1
64	4.44E-07	0.04007	1.04315	0.01003	9.34235	0.03176	157.3622	2.13E+29
73	4.38E-07	0.04292	0.96834	0.01367	8.08059	0.03224	146.5375	1.94E+20
82	4.38E-07	0.0431	1.01694	0.01318	8.54129	0.03015	140.0291	1.14E+18
91	4.31E-07	0.04469	1.00711	0.0143	7.70633	0.02605	145.4989	2.52E+16
100	4.32E-07	0.04643	0.63448	0.01541	8.22441	0.03112	139.3362	707.2279

Overcharge Overdischarge								
cycle #	L1 (H)	R1 (Ohm)	Q1 (F.s^(a - 1))	R2 (Ohm)	Q2 (F.s^(a - 1))	R3 (Ohm)	Q3 (F.s^(a - 1))	Q4 (F.s^(a - 1))
1	4.49E-07	0.03174	5.97087	0.01111	0.90485	0.01557	2.08E+23	373.8614
10	4.49E-07	0.03329	6.52856	0.0184	0.85453	0.0111	11523.34	324.4806
19	4.49E-07	0.03423	6.93791	0.02313	0.95974	0.00998	375552.5	243.1884
28	4.49E-07	0.03519	8.01721	0.02029	0.88105	0.00895	50039.46	186.3018
37	4.49E-07	0.03613	8.46619	0.02409	0.76512	0.00975	6.45E+17	184.2484
46	4.49E-07	0.03697	8.83581	0.02641	0.74915	0.01017	1.83E+59	162.6207
55	4.49E-07	0.03846	9.10805	0.02756	0.6667	0.00989	3.37E+39	154.0203
64	4.49E-07	0.04276	7.98188	0.02645	0.85095	0.01714	--	144.5542
73	4.49E-07	0.04632	7.40239	0.03051	0.47746	0.01504	--	163.1724

Appendix B. Neural network codes in python language

Code template acknowledgement:

https://www.kdnuggets.com/2018/10/simple-neural-network-python.html

```
from numpy import *
import numpy as np
import pandas as pd
import tkinter as tk
from tkinter import filedialog
import matplotlib.pyplot as plt
root= tk.Tk()
rawa = []
rawb = []
rawc = []
```

```
tempInputs=[]

tempOutputs=[]

a = []

b = []

c = []

d = []

canvas1 = tk.Canvas(root, width = 300, height = 300, bg = 'lightsteelblue2', relief = 'raised')

canvas1.pack()

headers = ['R1 (Ohm)','R2 (Ohm)','R3 (Ohm)']

aPercent=[]

bPercent=[]

cPercent=[]

aReal=[]

bReal=[]

cReal=[]

'''



'''

def getCSV ():

    '''

    NeuralNet Function Class

    Includes all Neural network util

    Main Function is defined as NeuralNet

    '''

    class NeuralNet(object):

        def __init__(self):
```

```
        random.seed(1)
        self.synaptic_weights = 2 * random.random((3, 3)) - 1
        # print(self.synaptic_weights)

    def __sigmoid(self, x):
        # return 1 / (1 + exp(-x))
        return tanh(x)
        # return np.where(x < 0, 0, x)

    def __sigmoid_derivative(self, x):
        # return x * (1 - x)
        return 1.0 - tanh(x) ** 2
        # return np.where(x < 0, 0, 1)

    # Train the neural network and adjust the weights each time.
    def train(self, inputs, outputs, training_iterations):
        for iteration in range(training_iterations):
            # Pass the training set through the network.
            output = self.learn(inputs)
            error = outputs - output
            # Adjust the weights by a factor
            factor = dot(inputs.T, error * self.__sigmoid_derivative(output))
            self.synaptic_weights += factor

    def learn(self, inputs):
        return self.__sigmoid(dot(inputs, self.synaptic_weights))
```

```
neural_network = NeuralNet()
global df
import_file_path = filedialog.askopenfilename()
firstin = pd.read_csv(import_file_path)
element = pd.DataFrame(firstin,columns=headers)
products_list = element.values.tolist()
#print(products_list)
for dataset in products_list:
    rawa.append(dataset[0])
    rawb.append(dataset[1])
    rawc.append(dataset[2])
for i in range(4):
    rawa.pop()
    rawb.pop()
    rawc.pop()


rawelem = [list(x) for x in zip(rawa,rawb,rawc)]
#print(rawelem)
realData = rawelem.pop()
#print(realData)
testcase = rawelem.pop()
#print(testcase)
if len(rawelem)%3!=0:
    if (len(rawelem) % 3 == 1):
        rawelem.pop()
```

```
        if (len(rawelem) % 3 == 2):
            rawelem.pop()
            rawelem.pop()
    print(len(rawelem))
    counter = 0
    for i in range(len(rawelem)):
        if(counter == 0):
            tempInputs.append(rawelem[i])
            counter +=1
        elif(counter ==1):
            tempInputs.append(rawelem[i])
            tempOutputs.append(rawelem[i])
            counter +=1
        elif(counter ==2):
            tempOutputs.append(rawelem[i])
            counter = 0
    inputs = array(tempInputs)
    outputs = array(tempOutputs)


    # We use first 3 inputs to predict the next 3 inputs.
    # We are using NCND files for input
    # numpy has variable array
    c.append(0)
    b.append(0)
    a.append(0)
    d.append(0)
```

```
listcontainer = []
for i in range(50):
    neural_network.train(inputs, outputs, 1000000)
    listcontainer.append(neural_network.learn(testcase).tolist())
    c.append(listcontainer[0].pop())
    b.append(listcontainer[0].pop())
    a.append(listcontainer[0].pop())
    listcontainer = []
    d.append(i + 1)
    print("After " + str(i + 1) + " million times training....")

aPercent.append(0)
bPercent.append(0)
cPercent.append(0)

for elem in a:
    if elem != 0:
        aPercent.append(abs((elem - realData[0])) / elem * 100)
for elem in b:
    if elem != 0:
        bPercent.append(abs((elem - realData[1])) / elem * 100)
for elem in c:
    if elem != 0:
        cPercent.append(abs((elem - realData[2])) / elem * 100)

aReal.append(0)
```

```
    bReal.append(0)
    cReal.append(0)
    for i in range(len(d) - 1):
        aReal.append(realData[0])
        bReal.append(realData[1])
        cReal.append(realData[2])
    # print(aPercent)
    # print(bPercent)
    # print(cPercent)
    lines = [a, b, c]
    colors = ['r', 'g', 'b']
    labels = ['R1-predicted', 'R2-predicted', 'R3-predicted']
    for i, g, l in zip(lines, colors, labels):
        plt.plot(d, i, g, label='l')
        plt.legend(labels)
        plt.ylabel('Resistance (Ohm)')
        plt.xlabel('Times (Millions)')
        plt.title("Predictions Vs Times")
    plt.show()


    lines = [aPercent, bPercent, cPercent]
    colors = ['r', 'g', 'b']
    labels = ['R1-percent-error', 'R2-percent-error', 'R3-percent-error']
    for i, g, l in zip(lines, colors, labels):
        plt.plot(d, i, g, label='l')
        plt.legend(labels)
```

```
        plt.ylabel('Machine Learning percent error (%)')
        plt.xlabel('Times (Millions)')
        plt.title("Percent error Vs Times")
    plt.show()


    lines = [a, aReal]
    colors = ['r', 'g']
    labels = ['R1-predicted', 'R1-experimental']
    for i, g, l in zip(lines, colors, labels):
        plt.plot(d, i, g, label='l')
        plt.legend(labels)
        plt.ylabel('Resistance (Ohm)')
        plt.xlabel('Times (Millions)')
        plt.title("R1 prediction Vs Times")
    plt.show()


    lines = [b, bReal]
    colors = ['r', 'g']
    labels = ['R2-predicted', 'R2-experimental']
    for i, g, l in zip(lines, colors, labels):
        plt.plot(d, i, g, label='l')
        plt.legend(labels)
        plt.ylabel('Resistance (Ohm)')
        plt.xlabel('Times (Million)')
        plt.title("R2 prediction Vs Times")
    plt.show()
```

```
    lines = [c, cReal]
    colors = ['r', 'g']
    labels = ['R3-predicted', 'R3-experimental']
    for i, g, l in zip(lines, colors, labels):
        plt.plot(d, i, g, label='l')
        plt.legend(labels)
        plt.ylabel('Resistance (Ohm)')
        plt.xlabel('Times (Million)')
        plt.title("R3 prediction Vs Times")
    plt.show()
browseButton_CSV = tk.Button(text="Import CSV File", command=getCSV, bg='green', fg='white',
font=('helvetica', 12, 'bold'))
canvas1.create_window(150, 150, window=browseButton_CSV)
root.mainloop()
#if __name__ == "__main__":
    # Initialize main function. Or redefine the main function to NeuralNet
```

Appendix C. Results for all four groups of tests using three activation functions

1. Normal charge normal discharge;

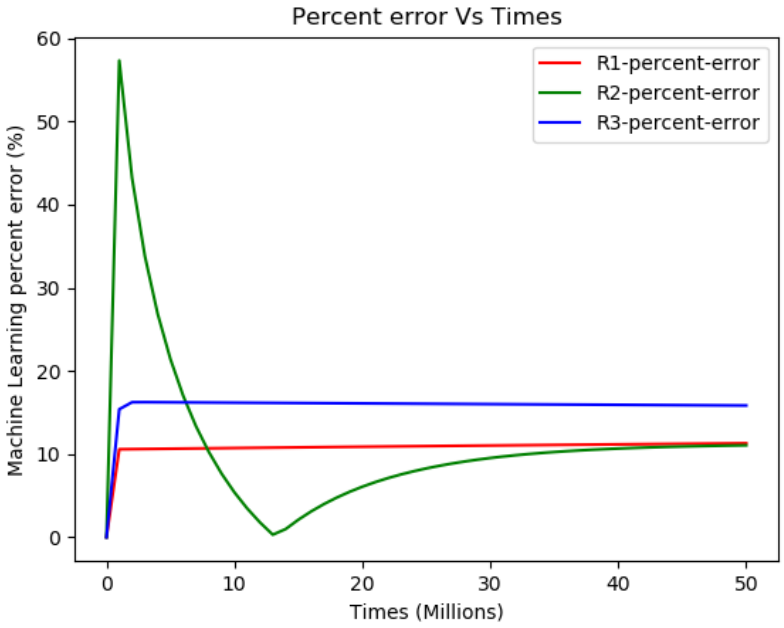

Sigmoid

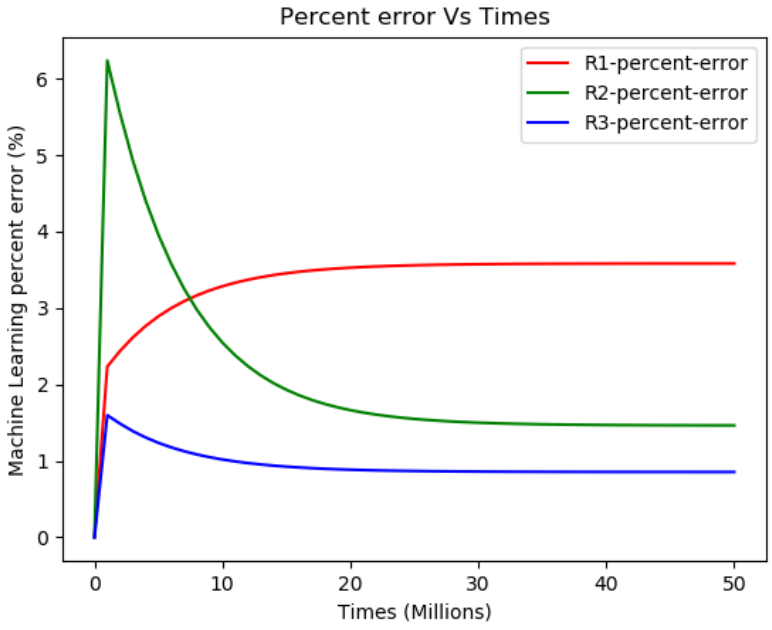

Tanh

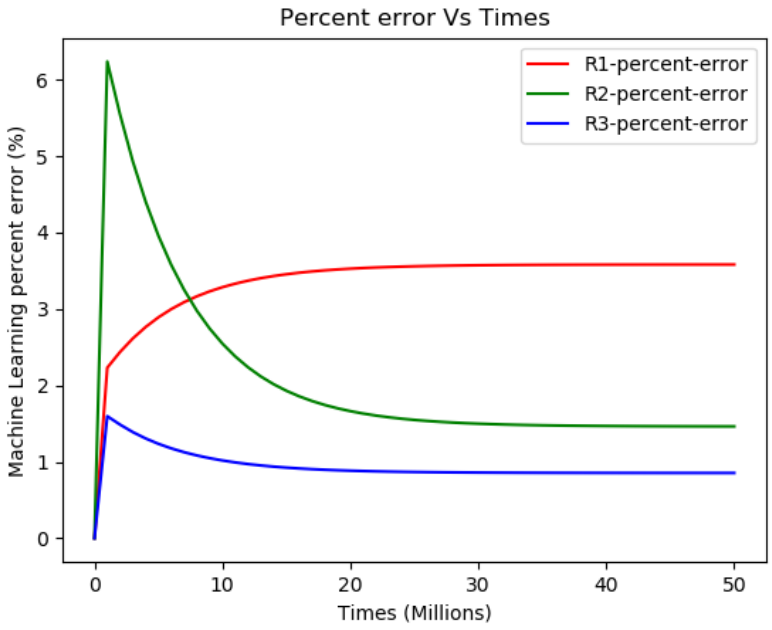

ReLu

2. Normal charge over discharge;

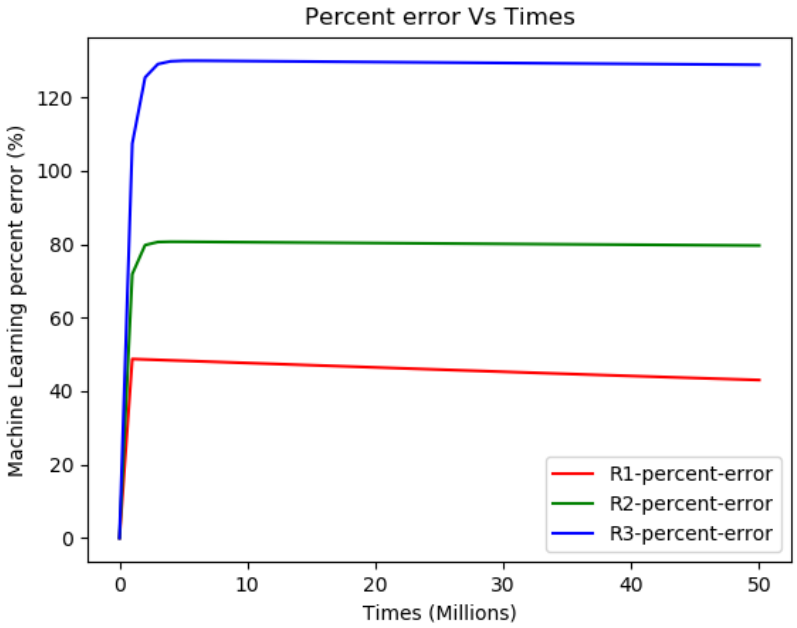

Sigmoid

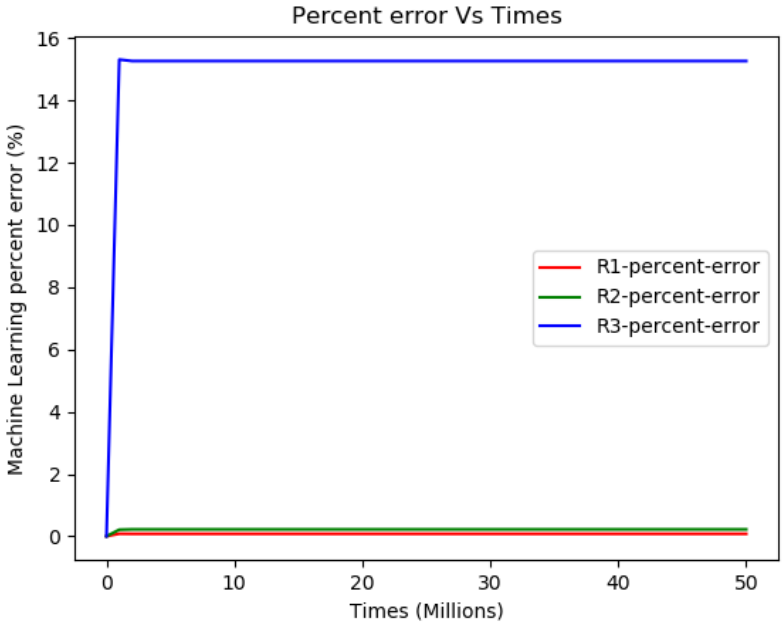
Percent error Vs Times
Machine Learning percent error (%)
Times (Millions)
R1-percent-error
R2-percent-error
R3-percent-error
0
2
4
6
8
10
12
14
16
0
10
20
30
40
50

Tanh

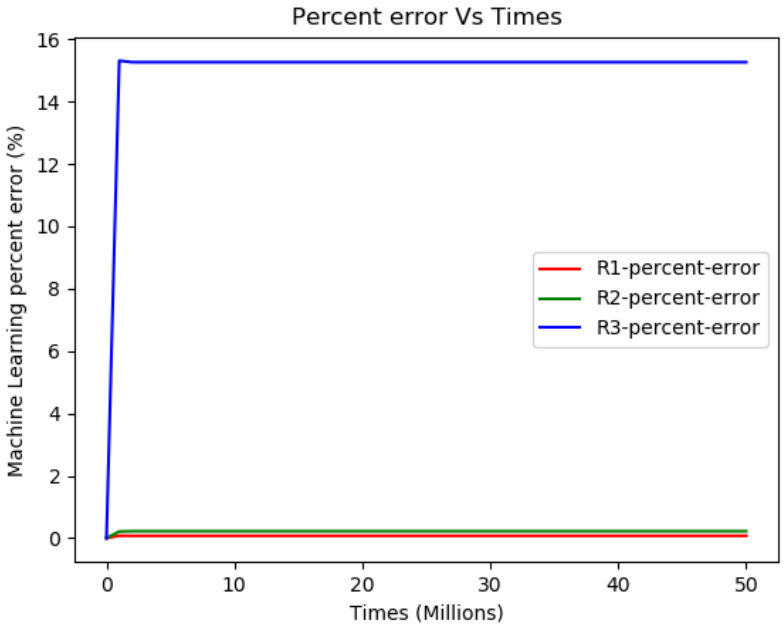
Percent error Vs Times
Machine Learning percent error (%)
Times (Millions)
R1-percent-error
R2-percent-error
R3-percent-error
0
2
4
6
8
10
12
14
16
0
10
20
30
40
50

ReLu

3. Over charge normal discharge;

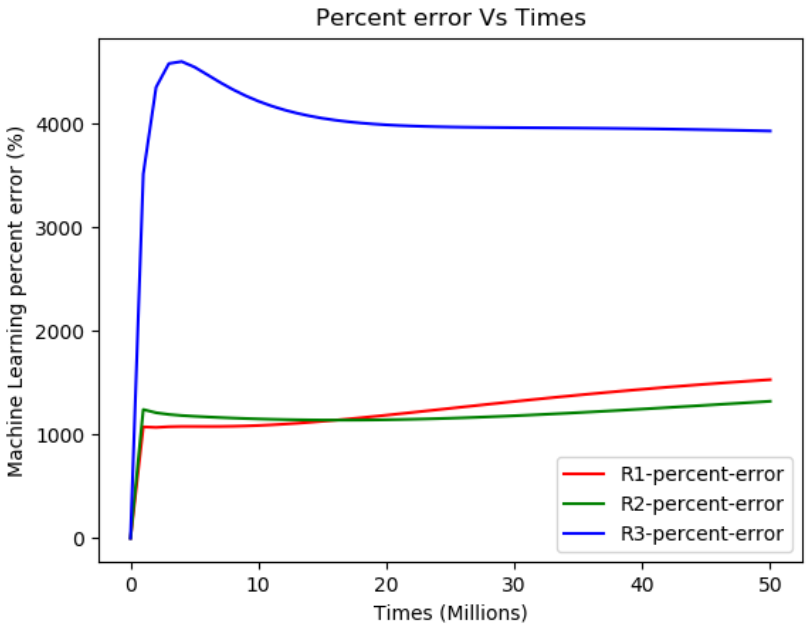

Sigmoid

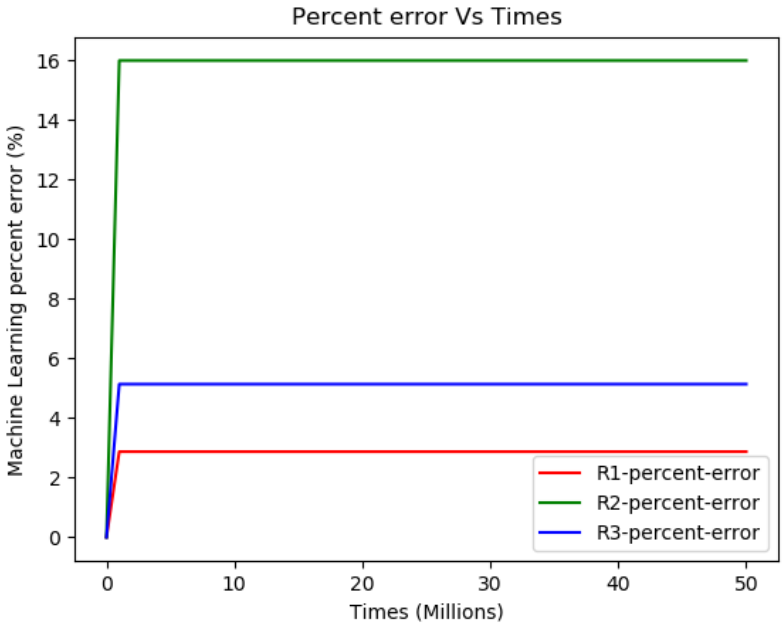

Tanh

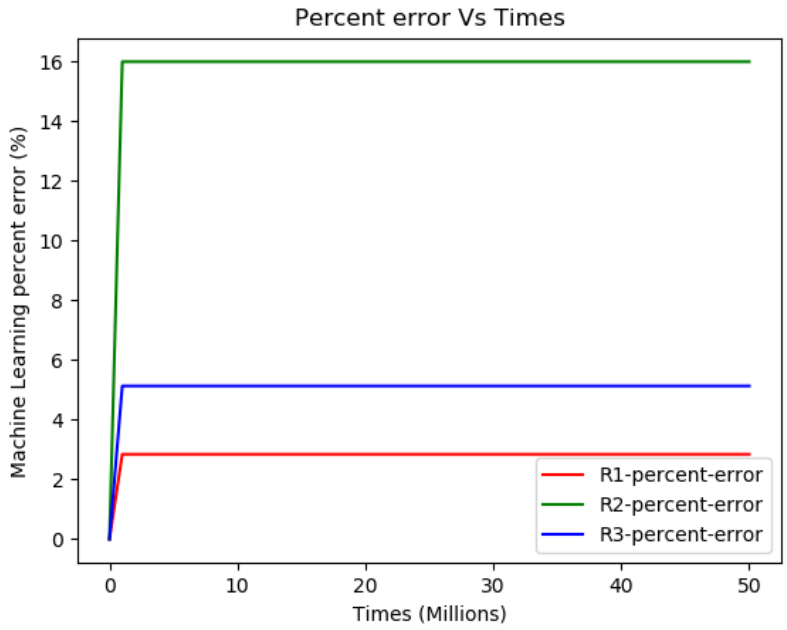

ReLu

4. Overcharge overdischarge.

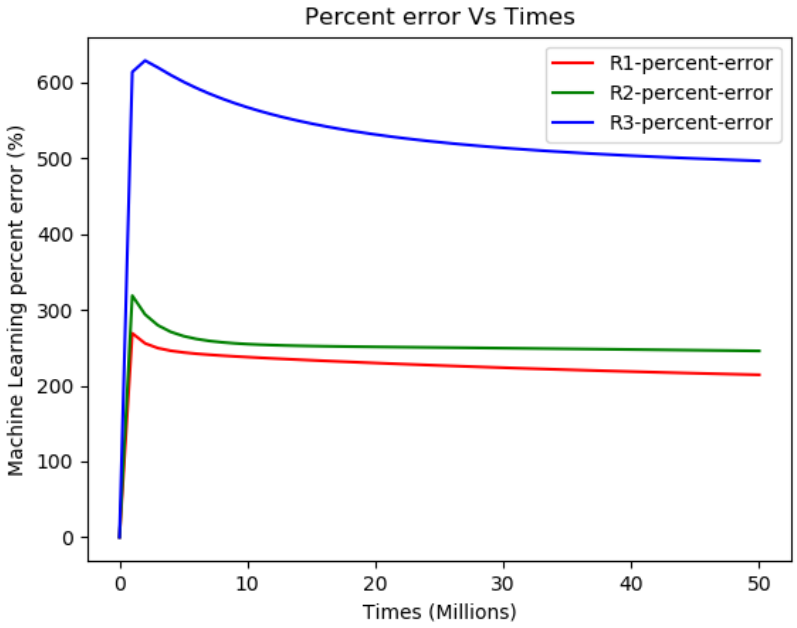

Sigmoid

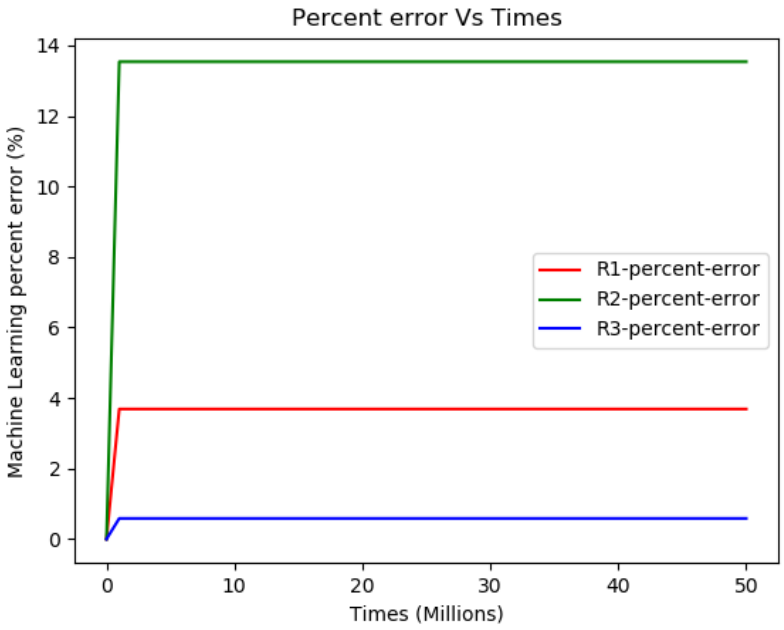
Percent error Vs Times
Machine Learning percent error (%)
Times (Millions)
R1-percent-error
R2-percent-error
R3-percent-error
0
2
4
6
8
10
12
14
0
10
20
30
40
50

Tanh

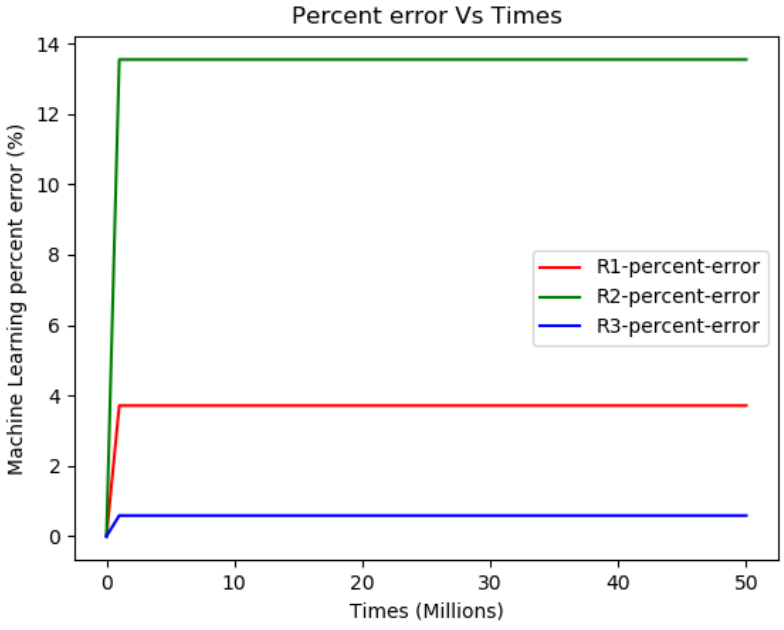
Percent error Vs Times
Machine Learning percent error (%)
Times (Millions)
R1-percent-error
R2-percent-error
R3-percent-error
0
2
4
6
8
10
12
14
0
10
20
30
40
50

ReLu